Received: 17 April 2017 | Revised: 23 January 2018 | Accepted: 27 January 2018

DOI: 10.1002/cne.24409

RESEARCH ARTICLE

WILEY JCN RESEARCH IN SYSTEMS NEUROSCIENCE THE JOURNAL OF COMPARATIVE NEUROLOGY

Immunolocalization of muscarinic M1 receptor in the rat medial prefrontal cortex

Satoko Oda[1] | Yousuke Tsuneoka[1] | Sachine Yoshida[1,2] | Satomi Adachi-Akahane[3] | Masanori Ito[3] | Masaru Kuroda[1] | Hiromasa Funato[1,4]

[1]Department of Anatomy, Faculty of Medicine, Toho University, Tokyo 143-8540, Japan

[2]Precursory Research for Embryonic Science and Technology (PRESTO), Japan Science and Technology Agency, Saitama 332-0012, Japan

[3]Department of Physiology, Faculty of Medicine, Toho University, Tokyo 143-8540, Japan

[4]International institute for integrative sleep medicine (IIIS), Tsukuba University, Ibaraki 305-8575, Japan

Correspondence
Satoko Oda, Department of Anatomy, Faculty of Medicine, Toho University, Tokyo, 143-8540, Japan.
Email: odas@med.toho-u.ac.jp

Funding information
Grant Sponsor: KAKENHI (Grants-in-Aid for Scientific Research) from the Ministry of Education, Culture, Sports, Science and Technology (MEXT) of Japan, Grant/Award Number: 15K08160 to SO, HF, and YT

Abstract

The medial prefrontal cortex (mPFC) has been considered to participate in many higher cognitive functions, such as memory formation and spatial navigation. These cognitive functions are modulated by cholinergic afferents via muscarinic acetylcholine receptors. Previous pharmacological studies have strongly suggested that the M1 receptor (M1R) is the most important subtype among muscarinic receptors to perform these cognitive functions. Actually, M1R is abundant in mPFC. However, the proportion of somata containing M1R among cortical cellular types, and the precise intracellular localization of M1R remain unclear. In this study, to clarify the precise immunolocalization of M1R in rat mPFC, we examined three major cellular types, pyramidal neurons, inhibitory neurons, and astrocytes. M1R immunopositivity signals were found in the majority of the somata of both pyramidal neurons and inhibitory neurons. In pyramidal neurons, strong M1R immunopositivity signals were usually found throughout their somata and dendrites including spines. On the other hand, the signal strength of M1R immunopositivity in the somata of inhibitory neurons significantly varied. Some neurons showed strong signals. Whereas about 40% of GAD67-immunopositive neurons and 30% of parvalbumin-immunopositive neurons (PV neurons) showed only weak signals. In PV neurons, M1R immunopositivity signals were preferentially distributed in somata. Furthermore, we found that many astrocytes showed substantial M1R immunopositivity signals. These signals were also mainly distributed in their somata. Thus, the distribution pattern of M1R markedly differs between cellular types. This difference might underlie the cholinergic modulation of higher cognitive functions subserved by mPFC.

KEYWORDS

astrocytes, GABAergic neurons, glia limitans, muscarinic receptor M1, prefrontal cortex, pyramidal neurons, RRID: AB_94856, RRID: AB_260731, RRID: AB_477329, RRID: AB_887884, RRID: AB_2109815, RRID: AB_2110656, RRID: AB_2278725, RRID: AB_2301751, RRID: SCR_003070

1 | INTRODUCTION

The prefrontal cortex (PFC) has been suggested to contribute in many cognitive functions, such as mnemonic processing, memory-guided behavior, spatial navigation, and motivated perception (de Bruin, Moita, de Brabander, & Joosten, 2001; Ethier, Rompré, & Godbout, 2001; Keil, 2004; Seamans, 2004; Carballo-Márquez et al., 2007; Shin & Jadhav, 2016). The entire cortical mantle including PFC is innervated by cholinergic afferents originating from the basal forebrain (BF), which consists of the nucleus basalis of Meynert, the substantia innominata, and the horizontal limb of the diagonal band (Wainer & Mesulam, 1990; Zaborszky et al., 2015). Moreover, cortical neuronal activity is regulated by these ascending cholinergic afferents (Steriade & Buzsáki, 1990; McCormick, 1992; Lucas-Meunier, Fossier, Baux, & Amar, 2003; Carballo-Márquez et al., 2007). Experimental lesions of rat BF impaired performance in spatial learning and target detection tasks (Browne, Lin,

Mattsson, Georgievska, & Isacson, 2001). The spatial memory performance of these animals was recovered by electrical stimulation of the degenerated BF (Lee, Jeong, Lee, Chang, & Chang, 2016). Similarly in humans, degeneration of BF is also associated with cognitive decline (Grothe, Heinsen, Amaro, Grinberg, & Teipel, 2016). These findings strongly suggest that cholinergic innervation is one of the important neuromodulators of the cognitive functions subserved by PFC. Therefore, anatomical evidence of the cholinergic system in PFC should lead to the advancement of understanding of these cognitive functions.

Muscarinic receptors are the metabolic type of acetylcholine receptors. They comprise five distinct subtypes, namely, M1 to M5. These muscarinic acetylcholine receptors are divided into two classes, M1-type receptors (M1, M3, and M5 receptors) and M2-type receptors (M2 and M4 receptors). M1-type receptors preferentially couple to the G-protein ($G_{\alpha q}$) and stimulate phospholipase C (PLC) leading to increased intracellular calcium concentrations. On the other hand, M2-type receptors couple to the G-protein ($G_{\alpha i}$) and inhibit adenyl cyclase activity as well as prolong potassium channel opening (Lucas-Meunier et al., 2003; Eglen 2012).

Among these five muscarinic receptors, the M1 receptor (M1R) is most abundant in the neocortex, as shown by both immunohistochemical and in situ hybridization analyses (Levey, Kitt, Simonds, Price, & Brann, 1991). A pharmacological study has demonstrated that benzylquinolone carboxylic acid (BQCA), a selective allosteric potentiator of M1R, increases the neuronal activity in the medial PFC (mPFC) in wild-type mice. No such an effect of BQCA was observed in M1R-KO mice (Shirey et al., 2009). Similarly, no acetylcholine effects on cortical pyramidal neurons, such as prolonged depolarization and spike acceleration, were observed in M1R-KO mice. On the other hand, the acetylcholine effects remained in pyramidal neurons of M3R-KO and M5R-KO mice (Gulledge, Bucci, Zhang, Matsui, & Yeh, 2009). Additionally, the functional binding of GTP to Gαq in the mouse cortex almost completely disappeared in M1R-KO mice (Felder et al., 2001). Thus, these acetylcholine effects may be predominantly mediated by M1R. M1R has been found in various cortical neuronal elements including both excitatory neurons (Mrzljak, Levey, & Goldman-Rakic, 1993; Disney, Domakonda, & Aoki, 2006; Yamasaki, Matsui, & Watanabe, 2010) and inhibitory neurons (Disney et al., 2006; Disney & Aoki, 2008; Disney & Reynolds, 2014). The distribution pattern of M1R-immunopositive somata in all cortical layers has been mainly examined in inhibitory neurons in the sensory cortices (Disney et al., 2006; Disney & Aoki, 2008; Disney & Reynolds, 2014). In these studies, the proportion of inhibitory neurons showing M1R immunopositivity signals highly varied among animal species and inhibitory neuronal subpopulations, and that of excitatory neurons showing M1R immunopositivity signals also highly varied among animal species and cortical areas. The intracellular localization pattern of M1R immunopositivity signals in cortical cells has been examined chiefly in excitatory neurons in monkeys and mice (Mrzljak et al., 1993; Disney et al., 2006; Yamasaki et al., 2010), and these ultrastructural studies were restricted in some cortical layers.

Therefore, we attempt to examine the distribution pattern of M1R-immunopositive somata of both pyramidal neurons and inhibitory neurons in all layers of rat PFC, and compare the intracellular localization pattern of M1R immunopositivity signals in pyramidal neurons with that in inhibitory neurons.

Additionally, previous studies have shown that astrocytes also contain M1R. For example, cultured astrocytes derived from the human brain were revealed to contain M1R by reverse transcription-polymerase chain reaction (RT-PCR) analysis (Elhusseiny, Cohen, Olivier, Stanimirović, & Hamel, 1999), and previous pharmacological analyses (Shelton & McCarthy, 2000, Chen et al., 2012) have shown that astrocytes in rat hippocampus and mouse primary visual cortex (V1) contain M1R.

However, only one immunohistochemical study has been carried out to show the immunolocalization of M1R/M2R in astrocytes (Chen et al., 2012). Astrocytes are categorized into some classes by morphology, function, and brain region. In the rodent cerebrum, three major types of astrocyte are identified (García-Marqués & López-Mascaraque, 2013; Liu et al., 2013; Tabata, 2015). First, protoplasmic astrocytes possessing highly branched processes are distributed in the grey matter. Second, fibrous astrocytes possessing straight and long processes are distributed in the white matter. Third, surface astrocytes (or pial astrocytes) located on the cortical surface form the glia limitans. Their somata are fibroblast-like shaped with bushy processes that are quite similar to those of protoplasmic astrocytes. Since we focused on the gray matter in this study, we examined the protoplasmic astrocytes and surface astrocytes.

To detect astrocytes, the glial fibrillary acidic protein (GFAP) and glutamine synthetase (GS) are commonly used as useful markers. GS immunopositivity signals are found in all cortical astrocytic somata, processes, perisynaptic buds, and end-feet surrounding vessels (Norenberg & Martinez-Hernandez, 1979; Robinson, 2001). GFAP immunopositivity signals are also found in all surface astrocytes and fibrous astrocytes. However, they are not detected in a subset of protoplasmic astrocytes. In the rat hippocampus, about 40% of cortical astrocytes were GFAP-immunonegative (Walz & Lang, 1998). GFAP-immunopositive astrocytes (GFAP astrocytes) and GFAP-immunonegative astrocytes are roughly distinguishable on the basis of their electrophysiological properties, cellular morphology, and other cellular markers (Jabs, Paterson, & Walz, 1997; Kimelberg, 2009). However, Zhou, Schools, and Kimelberg, (2000) have revealed by a single-cell RT-PCR analysis that majority of GFAP-immunonegative astrocytes possess GFAP mRNA. Additionally, the amounts of GFAP mRNA in cortices increase progressively during postnatal maturation (Nichols, Day, Laping, Johnson, & Finch, 1993) and reaction to an injury (Wilhelmsson et al., 2006; Yang & Wang, 2015). Furthermore, a large number of primary cultured astrocytes show GFAP immunopositivity signals (Kimelberg, 2009; Schildge, Bohrer, Beck, & Schachtrup, 2013). From these observations, GFAP astrocytes are considered mature and/or activated astrocytes (Kimelberg, 2009, 2010; Middeldorp & Hol, 2011, Schildge et al., 2013). In this study, to examine the proportion of M1R-immunopositive somata among mature astrocytes, we used GFAP as a marker. However, since GFAP immunopositivity signals cannot be detected in thin processes and perisynaptic buds, GS was also used to detect these small peripheral elements.

In this study, to examine the role of M1R in the rat PFC neural system, we compared the proportion of M1R-immunopositive somata and

TABLE 1 Information of primary antibodies

Antibody	Immunogen	Manufacture	Dilution
Muscarinic acetylcholine receptor (M1)	i_3 intracellular loop (aa 227–353) of human M1	Sigma-Aldrich; Rabbit polyclonal; Cat# M9808, RRID: AB_260731	1:500
67 kDa isoform of glutamic acid decarboxylase (GAD67)	N-terminus (aa 4–101) of human GAD67	Millipore; mouse monoclonal; Cat# MAB5406, RRID: AB_2278725 (Clone 1G10.2)	1:2,000
Parvalbumin (PV)	PV purified from frog muscle	Sigma-Aldrich; mouse monoclonal; Cat# P-3088, RRID: AB_477329 (Clone PARV-19)	1:4,000
Microtubule-associated protein-2 (MAP2)	Bovine brain microtubule protein (aa 997–1332)	Millipore; mouse monoclonal; Cat# MAB3418, RRID: AB_94856 (Clone AP20)	1:500
Vesicular glutamate transporter 1 (VGluT1)	C-terminus (542–560) of rat VGluT1	Millipore; guinea pig polyclonal; Cat# AB5905, RRID: AB_2301751	1:5,000
Vesicular glutamate transporter 2 (VGluT2)	C-terminus (510–582) of rat VGluT2	Synaptic Systems; guinea pig polyclonal; Cat# 135 404, RRID: AB_887884	1:1,000
Glial fibrillary acidic protein (GFAP)	GFAP purified from porcine spinal cord	Millipore; mouse monoclonal; Cat# MAB360, RRID: AB_2109815 (Clone GA5)	1:4,000
Glutamine synthetase (GS)	GS purified from sheep brain	Millipore; mouse monoclonal; Cat# MAB302, RRID: AB_2110656 (Clone GS-6)	1:500

the intracellular immunolocalization pattern of M1R between pyramidal neurons, inhibitory neurons, and astrocytes. Among the many cortical areas in rat PFC, we focused on the prelimbic cortex (PrL) in this study (Paxinos & Watson, 1998, Vogt, 2014). First, PrL in rodents is functionally analogous to primate lateral PFC, and it is involved in higher cognitive functions, such as initial acquisition and reversal learning (Birrell & Brown, 2000). Second, an atlas of in situ hybridization has demonstrated that M1R mRNA is densely distributed in rodent PrL (Allen Institute for Brain Science, 2004). Finally, M1R plays a crucial role in the early memory formation subserved by PrL (Carballo-Márquez et al., 2007).

2 | MATERIALS AND METHODS

2.1 | Animals

Eight male adult Sprague-Dawley rats (15 weeks old) weighing from 400 to 460 g were used in this study. The treatment and care of all the animals were approved by the Institutional Animal Care and Use Committee of Toho University (approved protocol ID 16- 52–286). The terminologies used for rat brain regions followed the atlas of Paxinos and Watson (1998).

2.2 | Antibodies and nuclear labeling

The following eight primary antibodies were used in this study (Table 1). The anti-M1R antibody is a rabbit polyclonal antibody against the third intracellular loop (aa 227–353) of human M1R. (Cat# M9808, RRID: AB_260731; Sigma-Aldrich, St. Louis, MO). This antibody was developed by Levey et al. (1991), and its specificity was confirmed by immunoblotting analysis, in which the anti-M1R antibody labeled a single band corresponding to the molecular weight predicted for M1R, and this band was distinct from other muscarinic receptors, namely, M2R to M5R.

The antibody to 67 kDa isoform of glutamic acid decarboxylase (GAD67) is a mouse monoclonal antibody against a recombinant his-tag-containing N-terminal region of human GAD67 (aa 4–101; Cat# MAB5406, RRID: AB_2278725, clone 1G10.2, Millipore, Temecula, CA) (Wang & Sun, 2012). GAD67 is a commonly used marker of inhibitory γ-aminobutyric acid (GABA)ergic neurons and widely distributed throughout the neuronal somata, thick dendrites, as well as axon terminals (Kaufman, Houser, & Tobin, 1991). The specificity of this anti-GAD67 antibody was previously confirmed by western blot analysis, in which the antibody labeled a single band of 67 kDa corresponding to the molecular weight of GAD67 (Wang & Sun, 2012).

The anti-parvalbumin (PV) antibody is a mouse monoclonal antibody against a purified frog muscle PV (Cat# P-3088, RRID: AB_477329, clone PARV-19; Sigma-Aldrich). This anti-PV antibody is derived from the PARV-19 hybridoma produced by the fusion between mouse myeloma cells and splenocytes from an immunized mouse. This antibody well labeled PV neurons in the reticular thalamus (Oda et al., 2014) but not the tissue of PV knockout mice (Burette, Strehler, & Weinberg, 2009).

The anti-microtubule-associated protein-2 (MAP2) antibody is a mouse monoclonal antibody against a bovine brain microtubule protein (aa 997–1332; Cat# MAB3418, RRID: AB_94856, clone AP20, Millipore). The specificity of this anti-MAP2 antibody was confirmed by western blot analysis, in which the antibody labeled a single band of approximately 280 kDa, roughly corresponding to the high-molecular-weight MAP2 isoforms MAP2a and MAP2b of about 280 kDa (Matsunaga et al., 1999). This antibody clearly labeled the dendrites and

somata of neurons in the avian nucleus laminaris (Tabor, Wong, & Rubel, 2011).

The anti-VGluT1 antibody is a guinea pig polyclonal antibody against a C-terminal domain (aa 542–560) of rat VGluT1 (Cat# AB5905; RRID:AB_2301751, Millipore; Melone, Burette, and Weinberg, 2005). The specificity of this anti-VGluT1 antibody was confirmed by western blot analysis, in which the antibody labeled a single band of 60 kD corresponding to the molecular weight of VGluT1 (Melone et al., 2005). The specificity was also tested by blocking the antiserum with the immunogen peptide (Wässle, Regus-Leidig, & Haverkamp, 2006). Melone et al. (2005) also performed double-immunolabeling experiments using the anti-VGluT1 antibody and another well-characterized anti-VGluT1 antibody (Bellocchio et al., 1998). As a result, they found the virtually complete overlapping of immunolabeling in the rat cerebral cortex. Furthermore, the anti-VGluT1 antibody used in the present study immunostained many synaptic puncta in control spinal cord sections. These VGluT1-immunopositive puncta were abolished in sections from VGluT1-KO animals (Siembab, Gomez-Perez, Rotterman, Shneider, & Alvarez, 2016).

The anti-VGluT2 antibody is a guinea pig polyclonal antibody against a purified recombinant protein corresponding to 73 amino acid sequence (aa 510–582) of rat VGluT2 (Cat# 135 404; RRID: AB_887884, Synaptic Systems). The anti-VGluT2 antibody immunolabeled the entire gray matter in the spinal cord (Siembab et al., 2016), and also the supragranular zone of the granule cell layer and the middle and outer molecular layers in the dentate gyrus (Perederiy, Luikart, Washburn, Schnell, & Westbrook, 2013). These immunolabeling patterns are quite similar to those in a previous study (Kaneko, Fujiyama, & Hioki, 2002) using a well-characterized anti-VGluT2 antibody (Fujiyama, Furuta, & Kaneko, 2001). Retinal ganglion cells including intrinsically photosensitive retinal ganglion cells (ipRGCs) contain VGluT2. The anti-VGluT2 antibody used in the present study effectively labeled retinal ganglion cells including ipRGCs in control mice but not in ipRGCs in mice with transgenetically deleted VGluT2 from ipRGCs (Purrier, Engeland, & Kofuji, 2014). We found that the anti-VGluT2 antibody immunolabeled all layers in mPFC. Among the layers, the immunopositivity signals of VGluT2 in the superficial part of layer I and the middle layer are stronger than those in other layers (data not shown). At a higher magnification, VGluT2-immunopositive axonal fiber- and terminal-like structures were distributed in neuropils (Figure 5e, f). This distribution pattern is also similar to that found in the study by Kaneko et al. (2002). Additionally, this distribution pattern is coincident with that of thalamocortical projections in mPFC (Rotaru, Barrionuevo, & Sesack, 2005).

The anti-GFAP antibody is a mouse monoclonal antibody against purified GFAP from the porcine spinal cord (Cat# MAB360, RRID: AB_2109815, clone GA5, Millipore). The specificity of this antibody was confirmed by western blot analysis, in which the antibody labeled a single band of approximately 51 kDa corresponding to the molecular weight predicted for GFAP (Buckman, Thompson, Moreno, & Ellacott, 2013). This antibody clearly labeled astrocytes in the hypothalamus (Buckman et al., 2013) and the posterodorsal medial amygdala (Johnson, Breedlove, & Jordan, 2013), as well as in the cochlear nucleus (Fuentes-Santamaría, Alvarado, Gabaldón-Ull, & Manuel Juiz, 2013).

The anti-GS antibody is a mouse monoclonal antibody against purified GS from the sheep brain (Cat# MAB302, RRID: AB_2110656, clone GS-6, Millipore). The specificity of this anti-GS antibody was confirmed by western blot analysis, in which the antibody labeled a single band of approximately 45 kDa, corresponding to the molecular weight predicted for GS (Chang, Wu, Jiang-Shieh, Shieh, & Wen, 2007). This antibody clearly labeled astrocytes in mouse mPFC (Kulijewicz-Nawrot, Syková, Chvátal, Verkhratsky, & Rodríguez, 2013) and Müller glia cells in the retina (Nasonkin et al., 2011).

For nuclear labeling, we used Hoechst 33342 (2 μg/ml, H21492; Molecular Probes, Eugene, OR), which produces light-blue fluorescence when it binds to DNA and is illuminated with UV light. Hoechst was mixed with a solution containing secondary antibodies (Kristensen, Noer, Gramsbergen, Zimmer, & Noraberg, 2003).

2.3 | Perfusion and sectioning

Anesthesia was induced with isoflurane and then the rats were deeply anesthetized with an overdose of urethane (over 1.2 g/kg body weight, i.p.: ethyl carbamate, Wako, Osaka) and perfused with 100 ml of 0.2% heparinized 0.1 M phosphate buffer (PB; pH 7.4), followed by 1,000 ml of a cold fixative solution containing 3% paraformaldehyde in 0.1 M PB through the ascending aorta. After perfusion, the brains were removed and postfixed for 3 hr in the fixative described above. Then, blocks of tissue specimens including mPFC were immersed in 20% sucrose in 0.1 M PB overnight before sectioning at a thickness of 60 μm with a freezing microtome. Sections were stored in a tissue cryoprotective solution (25% glycerol and 30% ethylene glycol in 0.05 M PB) at −80°C until use.

2.4 | Immunohistochemistry for light microscopy

The sections prepared for light microscopy were washed three times in phosphate-buffered saline (PBS; pH 7.2) and incubated for 5 days at 4°C on a shaker with the primary antibody against M1R in 0.1 M PBS containing 2% normal donkey serum. The sections were washed again in PBS and incubated overnight at 4°C on a shaker with a secondary antibody [biotinylated goat anti-rabbit IgG (BA-1000); Vector Laboratories, Burlingame, CA] at a dilution of 1:200 in PBS containing 2% normal donkey serum. They were then washed in PBS and incubated in an avidin-biotin-peroxidase complex solution (ABC kit; Vector Laboratories) overnight at 4°C on a shaker. They were washed again and incubated in 3,3′-diaminobenzidine (DAB; Sigma-Aldrich), which was diluted at 0.02% with PB containing 0.002% hydrogen peroxide and 0.02% $CoCl_2$ for enhancement, for 5–10 min at room temperature for visualization. The sections were mounted on gelatin-coated slides, dehydrated in a graded alcohol series, cleared with xylene, and coverslipped with Malinol (Muto Pure Chemicals, Tokyo, Japan). The sections were examined and photographed under a microscope (BX50; Olympus, Tokyo, Japan) equipped with a digital camera (DP70; Olympus).

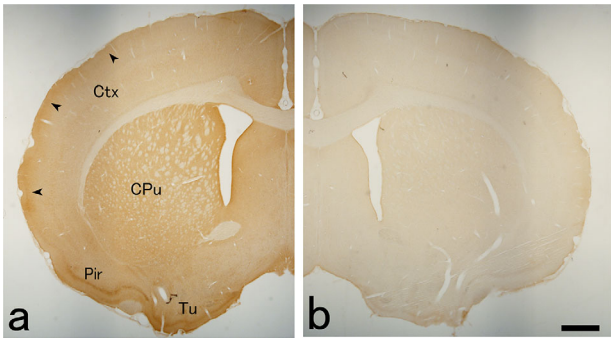

FIGURE 1 Photomicrographs of forebrain sections showing M1R immunopositivity signals in control section and in preadsorption section for anti-M1R antibodies. (a) Low-magnification image of control section. Strong M1R immunopositivity signals are found in Pir, Tu, and CPu. In the somatosensory cortices, the M1R-immunopositive superficial bands are also found (arrowheads). (b) Low-magnification image of preadsorption section. The M1R immunopositivity signal intensity is considerably lower than that of the control section (a). Scale bar = 1 mm in (b) (applies to a and b). Abbreviations: Ctx, cortex; CPu, caudate putamen; Pir, piriform cortex; Tu, olfactory tubercle

2.5 | Preadsorption experiments of anti-M1R antibody

Preadsorption experiments were carried out to check the specificity of the anti-M1R antibody. The M1R antigen (G043-mAChR-M1-AG, Frontier Institute, Japan) is a GST fusion protein, and its sequence corresponds to that of the mouse M1R (aa 229–358). Only one amino acid is different between mice and rats in the 227–358 aa sequence. The concentration of the antigen used was 50 μg/ml. For the preadsorption experiments, the anti-M1R antibody was dissolved in PBS containing the antigen for experimental sections or without the antigen for control sections. The final concentration of the anti-M1R antibody was 1:500. The PBS solutions containing the anti-M1R antibody with or without the antigen were allowed to stand for about 24 hr at 4°C before use, and then centrifuged at 12,000 rpm for 5 min. The resulting supernatants were used for light microscopy and confocal laser scanning microscopy.

The sections for light microscopy were processed in the same protocol as described above, and visualized by DAB staining without $CoCl_2$ for 5 min at room temperature. In the forebrain of a control section (Figure 1a), strong M1R immunopositivity signals were found in the piriform cortex (Pir), olfactory tubercle (Tu), and caudate putamen (CPu). In the somatosensory cortices, M1R immunopositive-bands were observed in the superficial layers. These immunolabeling patterns are quite similar to those observed in a previous paper (Levey et al., 1991). The signal intensity of M1R immunopositivity of the preadsorption section (Figure 1b) is considerably lower than that of the control section.

The sections for confocal laser scanning microscopy were processed in the same protocol as described below, but primary antibody was only anti-M1R antibody. Confocal microscopy showed that the signal intensity of M1R immunopositivity in the preadsorption sections was also considerably lower than that in control sections. The rate of decrease estimated using the profile view (ZEN ver. 2.3, Carl Zeiss, Oberkochen, Germany) is approximately 50% (data not shown).

2.6 | Immunohistochemistry for immunofluorescence experiments

The sections obtained for immunofluorescence experiments were washed three times in PBS and incubated for 5 days at 4°C on a shaker with a mixture of primary antibodies in 0.1 M PBS containing 2% normal donkey serum. The sections were washed again in PBS and incubated in a mixture of secondary antibodies [Alexa 555-conjugated donkey anti-rabbit IgG (A31572) for M1R detection, Alexa 488-conjugated donkey anti-mouse IgG (A21202) or Alexa 488-conjugated goat anti-mouse IgG (A11001) for GAD67, PV, MAP2, GFAP, and GS detection; Alexa 488-conjugated goat anti-guinea pig IgG (A11073) for VGluT1 and VGluT2 detection; 1:400; Molecular Probes] with 0.1 M PBS containing Hoechst and 2% normal donkey serum for 4 hr at room temperature. The sections were washed in PBS, then briefly washed in distilled water and mounted on slides with ProLong Diamond (Thermo Fisher Scientific, Waltham, MA).

2.7 | Confocal laser scanning microscopy

The sections were examined and photographed under an LSM-510 confocal laser scanning microscope (Carl Zeiss) equipped with a blue diode laser of 405 nm, an argon laser of 488 nm, and a HeNe laser of 543 nm. Hoechst 33342 fluorescence was viewed using a 420 nm longpass filter (Ch2), Alexa Fluor 488 fluorescence using a 505–530 nm BP filter (Ch3), and Alexa Fluor 555 fluorescence using a 561–636 nm filter (ChS1).

Images were obtained using the 100× oil immersion objective lens (NA, 1.4). For obtaining images, the pinhole size used for Alexa 555 was 172 μm. This size corresponds to an airy unit 1, which is the value recommended by Carl Zeiss. The thickness of the optical slices is 0.8 μm under this condition. For Alexa 488 and Hoechst (405), pinhole sizes were adjusted to 172 and 160, respectively, to obtain optical slices of 0.8 μm thickness.

For small somata (GAD67-, PV-, and GFAP-immunopositive cells), serial slices were obtained using Z-stacks at approximately 0.8 or 0.9 μm intervals. The brightness and contrast of images were adjusted using image browser software (ZEN2; Carl Zeiss). Then, images were exported to the TIFF format. The obtained images were assembled and additional lettering was incorporated in PaintShop Photo Pro X3 (Corel Corporation, Ottawa, Ontario, Canada). ImageJ (RRID: SCR_003070, NIH, Bethesda, MD) was only used for the changing color from red to magenta.

Images were obtained mainly in the intermediate and ventral areas at the caudal level of PrL. In these areas, it is easy to distinguish the borderline between PrL and the adjacent region, that is, the infra limbic cortex (IL), because layer II of IL is considerably thicker than that of PrL. Furthermore, the thickness of the cortex in these areas is smaller than

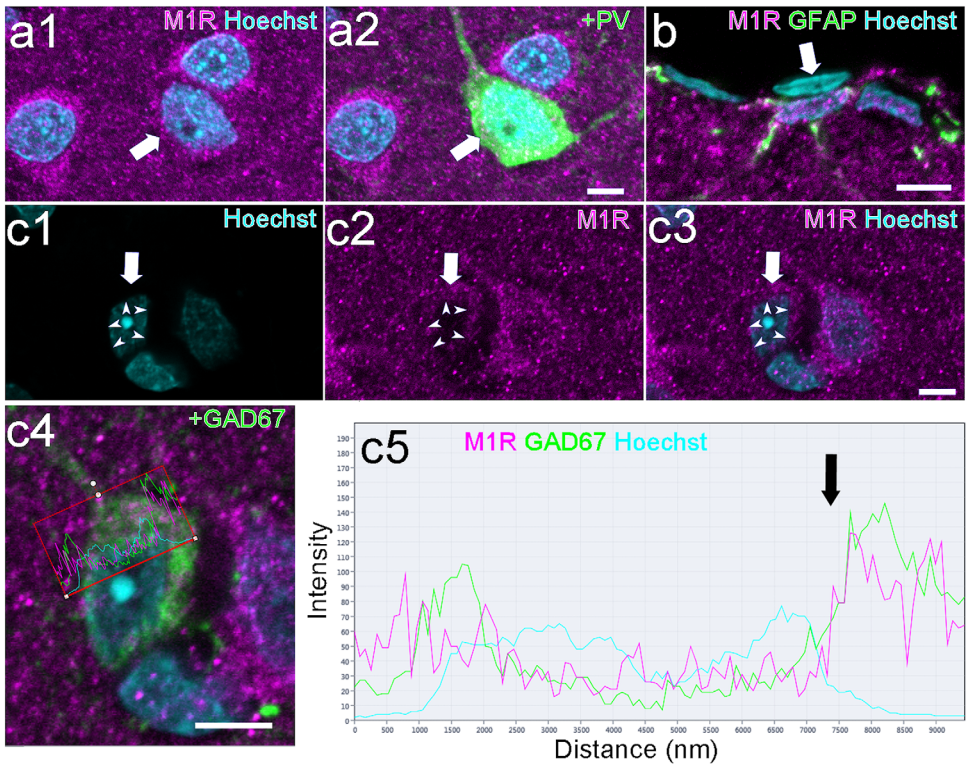

FIGURE 2 Examples of somata classified into strong, morderate, weak, and negative categories. (a) Three somata contain dots showing strong M1R immunopositivity signals. Among them, two somata are full of such dots. One PV neuron (indicated by arrow) contains apparently fewer such dots in somata. The formers are strong- and the latter is moderate-categories. (b) Example of Negative-category somata. No M1R immunopositivity signals are found around the nucleus of an endothelial cell (indicated by arrow). (c) Example of weak-category somata. A GAD67 neuron (indicated by arrow) contains only weak and faint M1R immunopositivity signals. (c1–3) The rim of the nucleus is indicated by arrowheads. The signals are located close to the rim of the nucleus. (c4 and 5) Profile views provide intensity profile graphs (0–255) of each channel image (c5) along a line (c4). (c5) The intensity of M1R immunopositivity signals is low in the nucleus, and it rises sharply at the rim of the nucleus (indicated by arrow). When such a pattern was observed in two or more Z-stack slices, the signals must be located in somata. One grid distance (pixel) is 0.09 μm. Magenta, M1R; Green; PV; Blue, Hoechst. Slice number of image/number of obtained Z-stack optical slices: (a) 3rd/5 slices, (b) 6th/11 slices, (c) 6th/10 slices. Scale bars = 5 μm in (a), (b), (c3) (applies to c1–c3), and (c4)

that in the rostral and dorsal areas. In confocal microscopy observation, the observation area was moved from the brain surface to the medulla side by a square unit (127.3 μm × 127.3 μm: objective lens 100×, electrical zoom 0.7). In each square, we observed somata that clearly show the nucleus and cellular markers at a higher magnification (objective lens 100×, electrical zoom 2–5).

Secondary antibodies have been tested. Only Alexa 555 donkey anti-rabbit IgG (H + L) may have a weak cross-reactivity to mouse IgG. No artifacts, however, were detected by visual inspection even under the condition of considerably high values of master gains. The maximum of the intensity of these artifacts under the condition was about 25 by profile view analysis. The value will be lower under usual conditions.

Because the intensity of M1R immunopositivity signals is over 100 even in somata in the weak category under usual conditions, these artifacts should not affect the classification of categories. In addition, immunopositivity signals of Alexa 555 and Alexa 488 are distinctly separated in neuropils (Figure 10c–e), and even within somata, the waveforms in each signal intensity graph constructed from the profile view are different (Figure 2c5).

2.8 | Category of M1R-immunopositive somata examined by confocal laser scanning microscopy

For counting M1R-immunopositive cells by confocal laser scanning microscopy, the signal strength of M1R immunopositivity in somata was classified into one of three categories as follows. (a) Strong–Moderate: A soma contains dots showing strong M1R immunopositivity signals. The pyramidal neuronal somata are usually full of such dots (Figure 2a). On the one hand, many of GAD- and PV-immunopositive neurons contain fewer such dots in somata (Figure 2a). The former was categorized into "Strong," and the latter was "Moderate." It was, however, difficult to distinguish between these categories in most cells. Thus, for statistical processing, they were combined into the category "Strong–Moderate." (b) Weak: A soma contains only weak and faint M1R immunopositivity signals (Figure 2c). (c) Negative: The M1R immunopositivity signals inside the soma cannot be identified. Usually, endothelial cells were M1R-immunonegative (Figure 2b).

Among these categories, "Weak" and "Negative" were difficult to distinguish in small somata, such as inhibitory neurons and astrocytes. Thus, we identified these somata on the basis of the following observations. (a) All sections were processed for nuclear staining, and all images

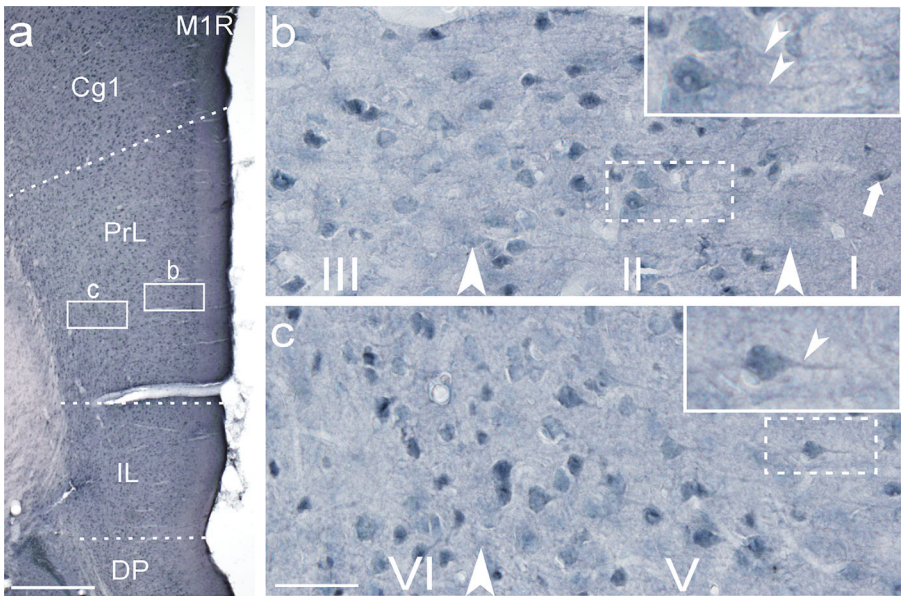

FIGURE 3 Photomicrographs of mPFC showing M1R immunopositivity signals. (a) Low-magnification image of mPFC. Dotted lines indicate the borderlines between cortical subregions. Framed areas in PrL are enlarged at a higher magnification in (b) and (c). (b) Superficial layers of PrL. Large arrowheads indicate the borderlines between layers I and II, and layers II and III. (c) Deep layers of PrL. A large arrowhead indicates the borderline between layers V and VI. Many M1R-immunopositive somata are found in layers II–VI. In layer I, a few M1R-immunopositive somata are observed. An example is indicated by an arrow in (b). Insets in (b) and (c) are obtained at a higher magnification of frames in (b) and (c), respectively. Because thick apical dendrites (small arrowheads) showing M1R immunopositivity signals are observed, these cells are identified as pyramidal neurons. Scale bars = 500 μm in (a), 50 μm in (c) (applies to b and c). Abbreviations: Cg1, cingulate cortex 1; IL, infralimbic cortex; DP, dorsal peduncular cortex

of small somata except one surface astrocyte were obtained using Z-stack slices. Nuclear staining was very useful. When immunopositivity signals located close to the nucleus are found in two or more Z-stack slices, this indicates that the soma contains intrasomal signals. The immunopositivity signals located in the peripheral region of somata were excluded, because they might be located in extrasomal regions. Somata with weak signals were examined visually and on the basis of their profile views. Profile views provide intensity profile graphs (0–255) of each channel image along a line. The signal intensities of M1R-immunopositive intracellular dots in pyramidal neurons and M1R-immunopositive puncta in neuropils were usually over 200. On the other hand, the signal intensity of M1R-immunopositive intracellular dots in weak-category somata usually did not exceed 150. An example is shown in Figures 2c4 and 5. The intensity of M1R immunopositivity signals is low in the nucleus and it rises sharply at the rim of the nucleus. When such a pattern was observed in two or more Z-stack slices, the signals must be located in somata. (b) In the case when the peak of the signal intensity of M1R-immunopositive dots is located in the middle slice in Z-stacks, this suggests that the dots are located in somata. From the above observations, particularly observation (a), we determined that the somata with weak signals are not M1R-immuninegative.

3 | RESULTS

3.1 | Light microscopy

In light microscopy at low-power magnification of M1R-immunopositive sections prepared by DAB-$CoCl_2$ labeling for visualization, many M1R-immunopositive somata were distributed throughout mPFC. At a higher magnification, M1R-immunopositive somata in PrL were mainly distributed in layers II–VI, and a few were also observed in layer I (Figure 3). It seems likely that a number of M1R-immunopositive cells are pyramidal neurons, as determined from their large somata and thick dendrites that vertically extend to the pia mater (insets in Figure 3b, c). Throughout the neuropils including layer I, many signals of M1R immunopositivity were widely distributed.

3.2 | M1R localization in pyramidal neurons

To examine the pyramidal neurons showing M1R immunopositivity signals, triple labeling using antibodies to M1R and GAD67, and the Hoechst stain were carried out. GAD67 is present exclusively in GABAergic neurons and their axon terminals (Kaufman et al., 1991). GAD67-immunonegative cells in the cerebral cortex are, however, not only excitatory neurons but also non-neuronal cells, such as glial and endothelial cells. Additionally, a previous paper has shown that a subset of GABAergic neurons shows no immunopositivity signals of GAD67 (Kadriu, Guidotti, Chen, & Grayson, 2012).

The standard criteria for the nuclear morphology of cortical glial cells in rats were well documented (Ling, Paterson, Privat, Mori, & Leblond, 1973; Ling & Leblond, 1973). According to their criteria, over 65% of all glial cells have smaller nuclei (mean diameter < 5.0 μm) than neurons. Only astrocytes and a subset of oligodendrocytes have larger nuclei (mean diameters, 6.3 and 7.0 μm, respectively). Among them, the nuclei of astrocytes characteristically show the distribution of

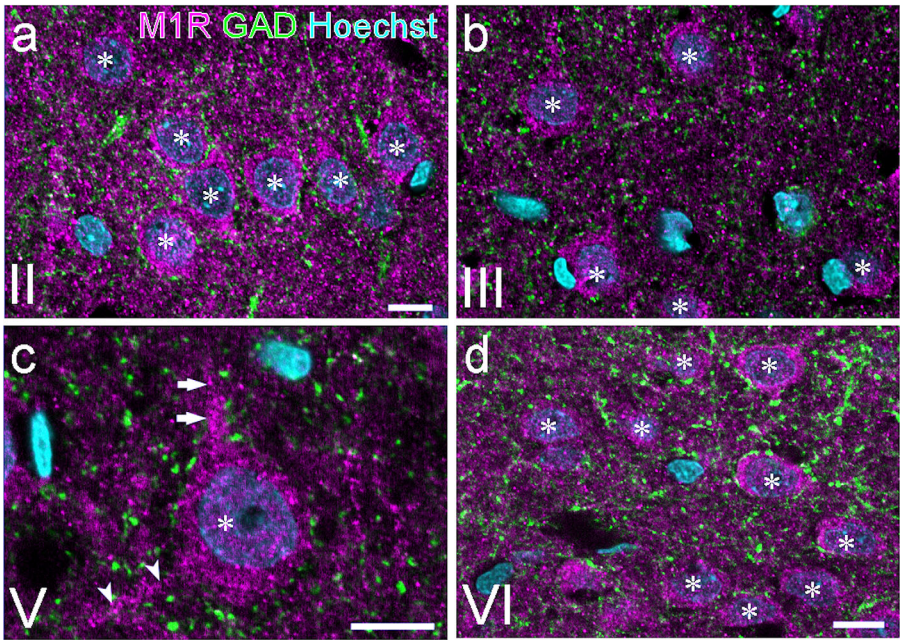

FIGURE 4 M1R immunopositivity signals in GAD67-immunonegative neurons in PrL visualized by confocal laser scanning microscopy showing triple labeling by antibodies to GAD67 (green) and M1R (magenta), and the Hoechst stain (blue). GAD67-immunonegative neurons showing M1R immunopositivity signals are found in layers II (a), III (b), V (c), and VI (d). Their somata (asterisks) are large, and the signals of M1R immunopositivity are uniformly strong. (c) A pyramidal neuron possessing M1R-immunopositive apical (arrows) and basal (arrowheads) dendrites. These images were obtained at 0.8 μm optical thickness. Slice number of image/number of obtained Z-stack optical slices: (a) 4th/7 slices, (b) single slice, (c) 2nd/4 slices, (d) 3rd/5 slices. Scale bars = 10 μm in (a) and (d) (applies to b and d), 5 μm in (c)

chromatin that follows the outline of the nuclei. The nuclei of a subset of oligodendrocytes are similar to those of neurons. However, they are distinctly few in number. In the rat cortex, they are only 0.3–0.7% of the total number of glial cells. In addition, endothelial cells characteristically have elongated nuclei that are intensely and uniformly labeled by the Hoechst stain.

Thus, we examined somata on the basis of the following criteria to exclude these glial cells and endothelial cells from the somata to be examined: (a) the nuclear diameter is more than 5 μm, (b) the nuclear staining is not uniformly intense, and (c) the nuclear staining does not clearly show the outline of the nucleus. Among these cells in layers II–V, somata that have apical dendrites, and are surrounded by GAD67-immunopositive puncta, that is, GABAergic inhibitory axon terminals, are considered to be those of pyramidal neurons, because pyramidal neurons are usually surrounded by dense GABAergic terminals derived from basket cells.

At a low magnification in triple labeling experiments, most pyramidal neurons showed M1R immunopositivity signals (Figures 4a, b, 5a). They had large somata and thick apical dendrites extending toward the pia mater. Some M1R-immunopositive basal dendrites were also observed (Figure 4c). Because the cytoplasmic region between the nucleus and the GAD67-immunopositive axon terminals was filled with many M1R-immunopositive dots, the shape of the nucleus was clearly recognizable. Furthermore, the nucleolar region was also clearly recognizable as an M1R-immunonegative region, because it is devoid of such dots (Figure 4c). Thus, the nucleolar region, as well as capillaries, is a useful benchmark for immunonegativity during the adjustment of brightness under a microscope. The qualitative impression was that most of the pyramidal neurons in layers II–V showed Strong–Moderate M1R immunopositivity signals.

In layer VI, most of the GAD67-immunonegative neurons showing M1R immunopositivity signals were also found, and they were not pyramidal in shape. Their dendrites were thinner and oriented in various directions (Figure 4d).

In the neuropils of all layers, numerous M1R-immunopositive puncta were observed. They were GAD67-immunonegative, round, and relatively uniform in size, and exhibited strong signals of M1R immunopositivity (Figure 5). To examine these puncta showing M1R immunopositivity signals, triple labeling of sections with the antibodies to M1R and one of following neuronal markers (MAP2, VGluT1, and VGluT2), and with the Hoechst stain was carried out. MAP2 is a microtubule-associated protein, and it is usually used for detecting dendritic shafts (Dehmelt & Halpain, 2004). At a low magnification, many MAP2-immunopositive apical dendrites originating from many pyramidal neurons were also M1R-immunopositive. These dendrites branched in layer I and formed dendritic tufts (Figure 5a).

In all VGluT1- or VGluT2-immunopositive presynaptic axon terminals, no signals of M1R immunopositivity were detected (Figure 5b–f). At a higher magnification, the axon terminals were often in the close vicinity of M1R-immunopositive puncta. The diameter of the puncta was roughly estimated to be 0.5 μm. As we will describe later, these puncta were not perisynaptic buds of astrocytes. Furthermore, it was

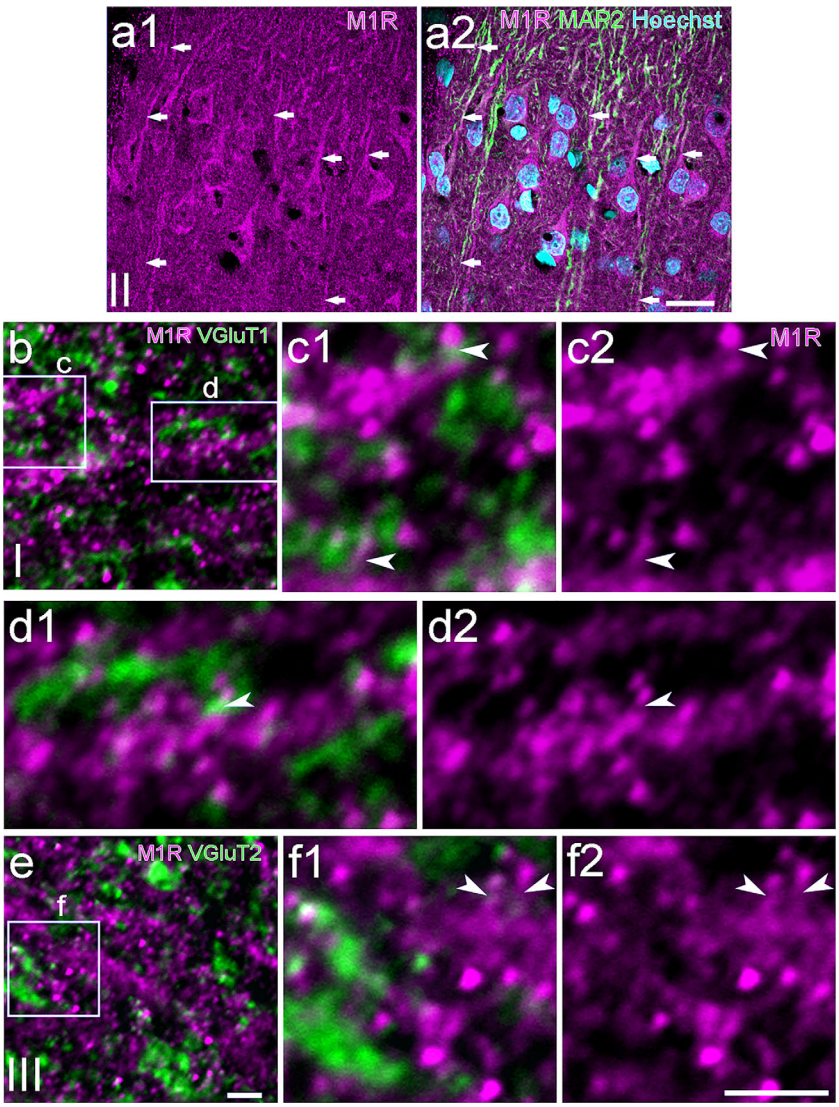

FIGURE 5 M1R immunopositivity signals in neuropils in PrL visualized by confocal laser scanning microscopy showing triple labeling by antibodies to neuronal markers (green), M1R (magenta), and the Hoechst stain (blue). (a) Many thick MAP2-immunopositive apical dendrites in layer II are also M1R-immunopositive. Arrows indicate double-immunopositive apical dendrites. (b) Higher magnification of the neuropil in layer I of VGluT1- and M1R-immunopositive section. (c) and (d) Enlarged images of framed areas in (b). (e) Higher magnification of the neuropil in layer III of VGluT2- and M1R-immunopositive section. (f) Enlarged images of framed area in (e). Both VGluT1- (b–d) and VGluT2- (e and f) immunopositive axon terminals are often found in close vicinity of M1R-immunopositive puncta. No double-immunopositive puncta are observed. It is also found that M1R-immunopositive puncta are connected to dendrites via small processes (indicated by arrows in c, d, and f). They appear like synaptic spines derived from dendritic shafts of pyramidal neurons. The signal intensity of M1R immunopositivity is higher in heads than that in necks of dendritic spines. Slice number of image/number of obtained Z-stack optical slices: (a–d) single slices, (e and f) 3rd/4 slices. Scale bars = 20 μm in (a), 2 μm in (e) (applies to b and e) and (f) (applies to c, d, and f)

often found that M1R-immunopositive puncta were connected to dendrites via small processes. Thus, they appeared like synaptic spines derived from dendritic shafts of pyramidal neurons. The signal intensity of M1R immunopositivity was higher in heads than that in necks of dendritic spines.

These findings are consistent with previous studies by electron microscopy. In the primate frontal cortex, many M1R-immunopositive dendritic spines were observed (Mrzljak et al., 1993). About 60% of dendritic spines were M1R-immunopositive in the rat basolateral amygdala (Muller, Mascagni, Zaric, & Mcdonald, 2013). Similarly, Yamasaki et al. (2010) have shown that M1R is detected in many dendritic spines as well as dendritic shafts in the mouse neocortex and hippocampus.

3.3 | M1R localization in inhibitory neurons

To examine the GABAergic inhibitory neurons showing M1R-immunopositivity signals, the sections were triple labeled with antibodies to M1R and GAD67, and the Hoechst stain. Because cortical GABAergic neurons are relatively small, we examined them using 3–12 Z-stack serial slices (0.8 μm optical thickness of Z-stacks). GAD67-

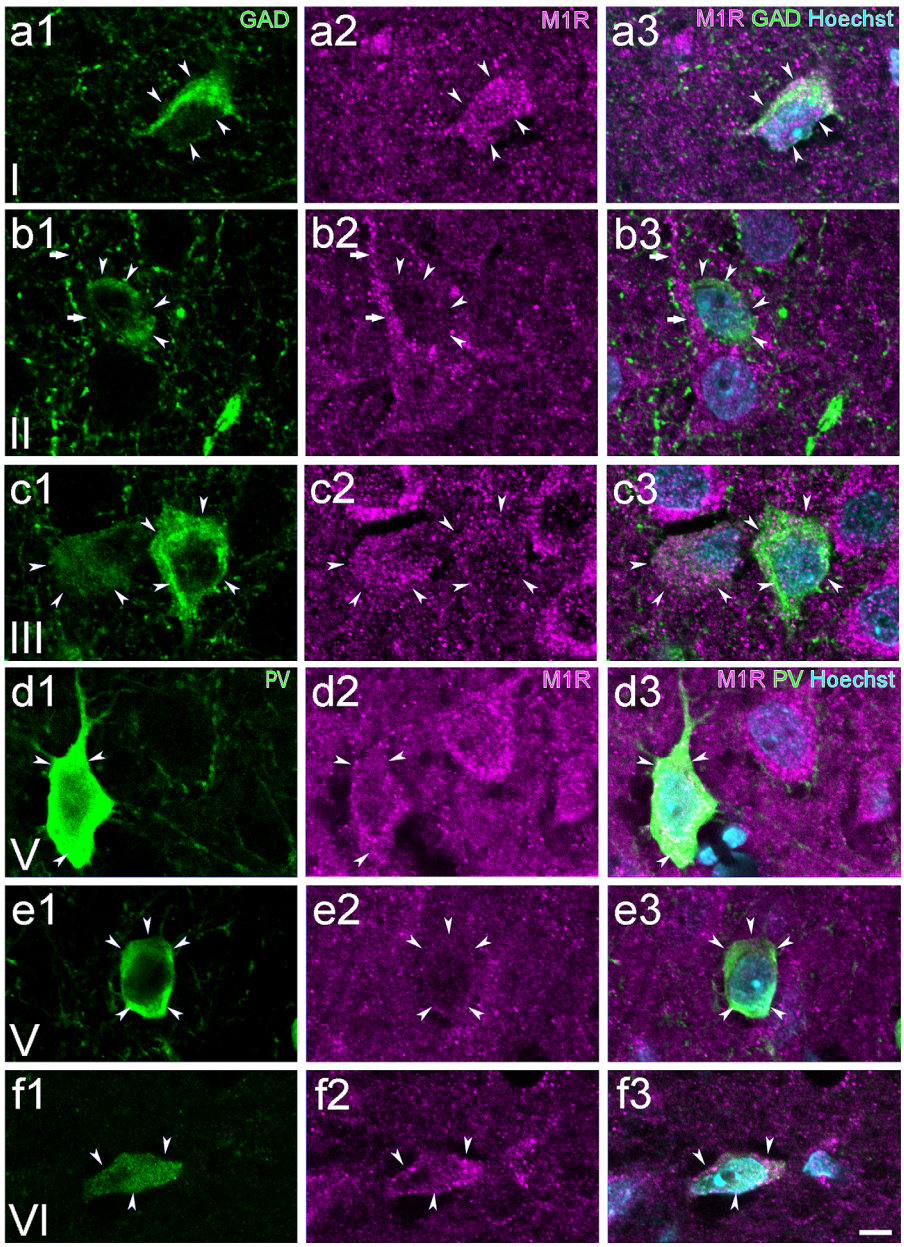

FIGURE 6 M1R immunopositivity signals in inhibitory neurons in PrL visualized by confocal laser scanning microscopy showing triple labeling by antibodies to GAD67 (a–c) or PV (d–f) (green), and M1R (magenta), and the Hoechst stain (blue). Arrowheads indicate neuronal somata. (a–c) GAD67- and M1R-immunopositive neurons are found in all layers. Examples in layers I (a), II (b), and III (c) are shown. The signal strength of M1R immunopositivity in their somata is not uniform. GAD67-immunopositive somata showing "Strong" (a, c left), "Moderate" (c right), and "Weak" (b) signals of M1R immunopositivity are observed. (d–f) PV- and M1R-immunopositive neurons are found in layers II–VI. Examples in layers V (d and e) and VI (f) are shown. The signal strength of M1R immunopositivity in their somata is not uniform, similarly to GAD67 neurons (a–c). PV-immunopositive somata showing "Strong" (d and f) and "Weak" (e) signals of M1R immunopositivity are observed. These images were obtained at 0.8 μm optical thickness. Slice number of image/number of obtained Z-stack optical slices: (a) 2nd/5 slices, (b) 3rd/4 slices, (c) 5th/12 slices, (d) 3rd/6 slices, (e) 3rd/5 slices, (f) 2nd/5 slices. Scale bars = 5 μm in (f) (applies to a–f)

immunopositive neurons (GAD67 neurons) were distributed throughout all layers in PrL (Figure 6a–c). Strong M1R immunopositivity signals were found throughout the somata and dendrites of many pyramidal neurons, described above. In GAD67 neurons, the signal strength of M1R immunopositivity varied among neurons. About 44% of GAD67 neurons showed "Strong–Moderate" signals, and an approximately equal proportion of neurons showed "Weak" signals of M1R immunopositivity (Figure 7). Thus, the signals of M1R immunopositivity were detected in approximately 88% of GAD67 neurons. The remaining GAD67 neurons were categorized into "Negative." The proportion of GAD67 neurons showing "Strong–Moderate" signals of M1R-immunopositivity in layer V was significantly higher than that in layers I, II, and VI (Figure 7). No M1R immunopositivity signals were detected in GAD67-immunopositive axonal terminals.

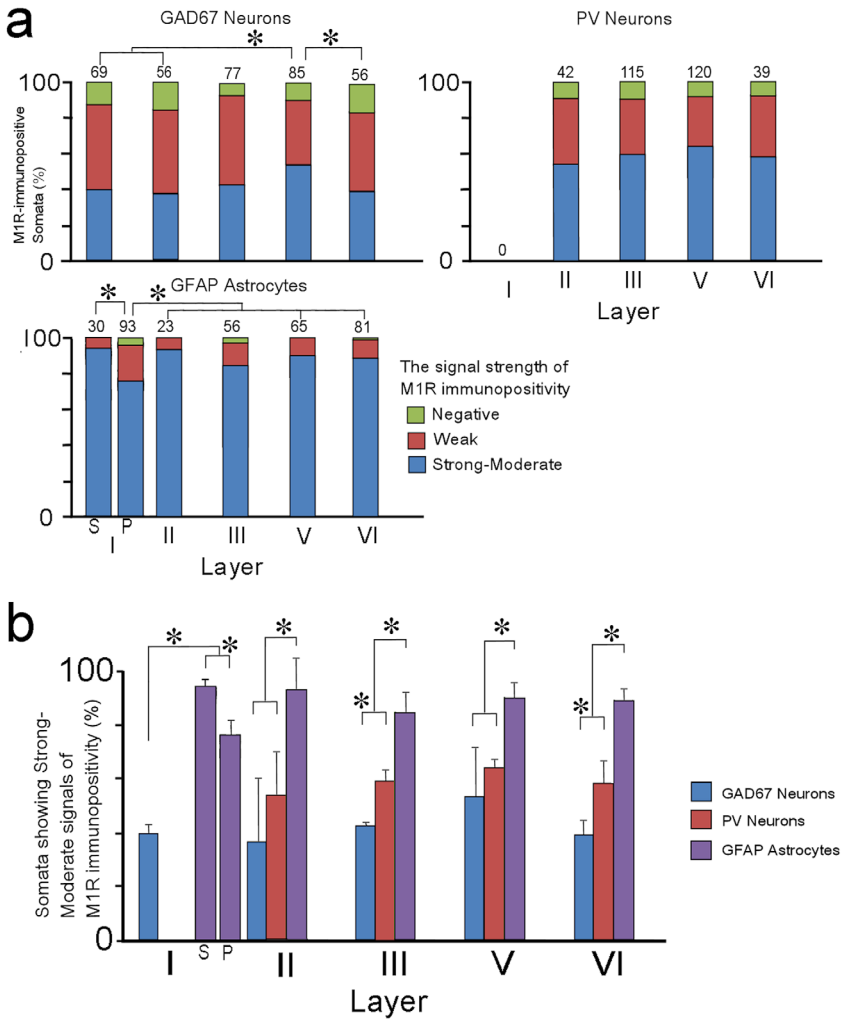

FIGURE 7 The proportion of somata containing M1R among cortical cellular types. (a) Mean percentages of M1R-immunopositive somata among GAD67 neurons, PV neurons, and GFAP astrocytes in layers I, II, III, V, and VI. Total numbers of counted cells obtained from three rats are given above. In layer I, two types of GFAP astrocytes, the surface astrocytes (S) and the protoplasmic astrocytes (P), are present. In other layers, all GFAP astrocytes are protoplasmic astrocytes. The signal strength of M1R immunopositivity in a soma is categorized into three groups as follows. Strong–Moderate: A soma contains dots showing strong signals of M1R immunopositivity. Pyramidal neuronal somata are usually full of such dots. Weak: A soma contains only weak and faint signals of M1R immunopositivity. Negative: The M1R-immunopositivity signals inside the soma cannot be identified. Significant differences in the proportion of somata showing "Strong–Moderate" signals of M1R immunopositivity between layers were assessed by Mann–Whitney's *U*-test. Asterisks (*) indicate $p < .05$. (b) Mean percentages of somata showing "Strong–Moderate" signals of M1R immunopositivity among GAD67 neurons, PV neurons, and GFAP astrocytes in layers I, II, III, V, and VI. Vertical bars indicate SD ($n = 3$ rats). Significant differences in the data between cellular subgroups in each layer were assessed by Mann–Whitney's *U*-test. Asterisks (*) indicate $p < .05$

PV-immunopositive neurons (PV neurons) showing M1R immunopositivity signals were also observed by triple labeling with the antibodies to M1R and PV, and the Hoechst stain. The cortical PV neurons were examined using 3–10 Z-stack serial slices (0.8 μm optical thickness of Z-stacks). In the cerebral cortex, PV neurons are the major component of GABAergic interneurons (Kubota, Hattori, & Yui, 1994). They are distributed in layers II–VI, and the signals of PV immunopositivity were widely distributed in their somata and throughout their dendrites, as well as axonal fibers and terminals. Examples of PV neurons showing M1R immunopositivity signals are shown in Figure 6d–f. The signal strength of M1R immunopositivity in PV neurons varied among neurons as in the case of GAD67 neurons. About 61% of PV neurons showed "Strong–Moderate" signals, and approximately 31% of the neurons showed "Weak" signals of M1R immunopositivity (Figure 7). Thus, the signals of M1R immunopositivity were detected in approximately 92% of PV neurons. The proportion of somata showing "Strong–Moderate" signals of M1R-immunopositivity was not significantly different between cortical layers except for layer I where PV neurons are absent (Figure 7).

Because PV immunopositivity signals were distributed throughout the dendrites of PV neurons, we examined the intradendritic localization pattern of M1R. The dendrites of 14 PV neurons were examined using 3–9 Z-stack serial slices (0.8 μm optical thickness of Z-stacks). Two examples are shown in Figure 8. The density of the intradendritic

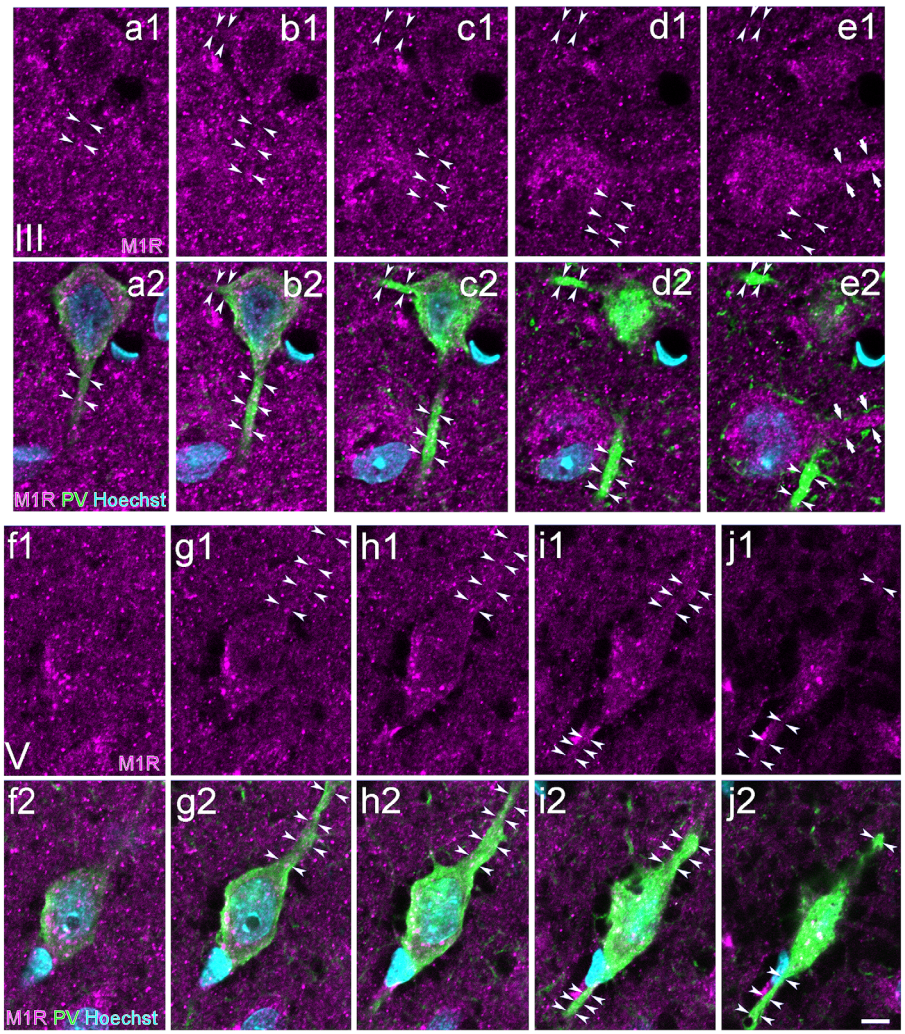

FIGURE 8 Intradendritic signals of M1R immunopositivity in PV neurons in PrL visualized by confocal laser scanning microscopy of Z-stack serial slices showing triple labeling by antibodies to PV (green) and M1R (magenta), and the Hoechst stain (blue). (a–e) and (f–j): Serial slices of thick dendrites (arrowheads) originating from PV-immunopositive somata in layers III and V, respectively. The signals of M1R immunopositivity in the dendrites are apparently weaker than those in the somata. In contrast, a dendrite (arrows in e) of a pyramidal neuron shows "Strong" signals of M1R immunopositivity. These serial slices (intervals, 0.8 μm) were obtained at 0.8 μm optical thickness of Z-stacks. Slice number of image/number of obtained Z-stack optical slices: (a–e) 5th–1st/7 slices, respectively, (f–j) 5th–1st/6 slices, respectively. Scale bars = 5 μm in (j) (applies to a–j)

signals of M1R immunopositivity greatly decreased from the somata to the distal region. This distribution pattern in PV neurons is quite different from that in pyramidal neurons, as described previously.

3.4 | M1R localization in astrocytes

To examine the GFAP astrocytes showing M1R immunopositivity signals, triple labeling with antibodies to M1R and GFAP, and the Hoechst stain were carried out. Because the somata of cortical astrocytes are smaller than those of neurons, we examined most of them using 3–11 Z-stack serial slices (0.8 μm optical thickness of Z-stacks). The protoplasmic GFAP astrocytes were distributed throughout cortical layers. M1R immunopositivity signals were found mainly at the site where nucleus and GFAP-immunopositive structures are in contact, and they were apparently weaker in their processes (Figure 9a–c). About 78% of protoplasmic GFAP astrocytes showed "Strong–Moderate" signals, and approximately 12% showed "Weak" signals of M1R immunopositivity (Figure 7). Thus, the signals of M1R immunopositivity were detected in approximately 90% of protoplasmic GFAP astrocytes. The proportion of the protoplasmic GFAP astrocytes showing "Strong–Moderate" signals of M1R immunopositivity in layer I was significantly lower than that in layers II, V, and VI (Figure 7). Sometimes, M1R-immunopositive puncta were observed along GFAP-immunopositive processes, but the processes of astrocytes are thin and GFAP is not a cytosolic marker, so it was difficult to distinguish between the inside and outside areas of the processes.

The glia limitans of rodents is located immediately below the pia mater and composed of another type of GFAP astrocyte, namely, surface astrocytes (Figure 9d, e). These surface astrocytes have been examined by electron microscopy (Liu et al., 2013) and in

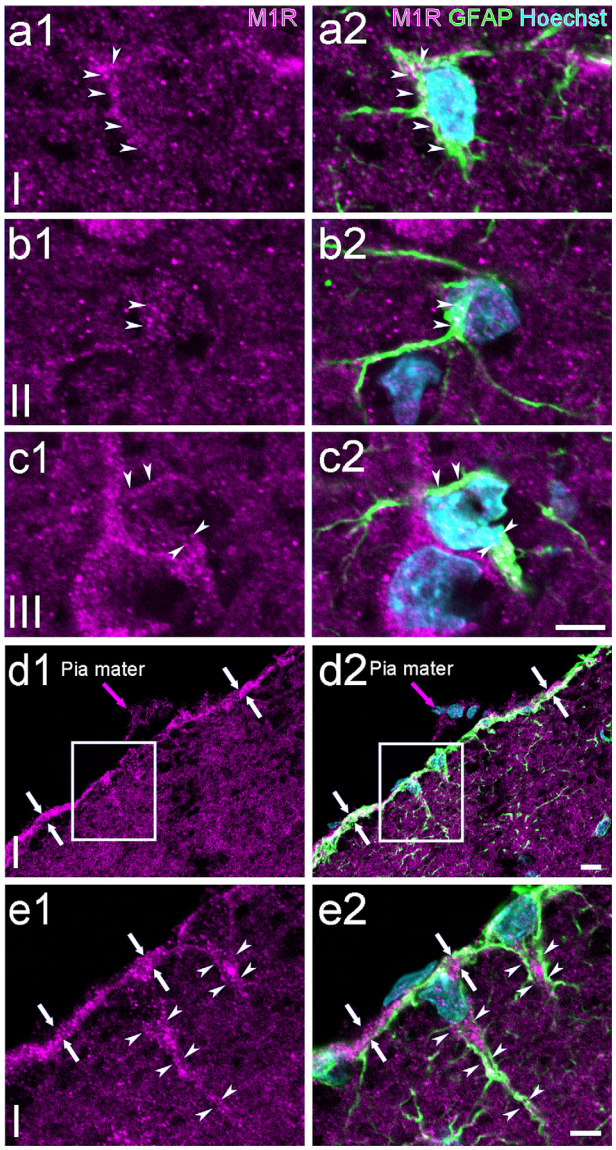

FIGURE 9 M1R immunopositivity signals in GFAP astrocytes in PrL visualized by confocal laser scanning microscopy showing triple labeling by antibodies to GFAP (green) and M1R (magenta), and the Hoechst stain (blue). (a–c) GFAP- and M1R-immunopositive astrocytes are found in all layers. Examples in layers I (a), II (b), and III (c) are shown. The signals of M1R immunopositivity are mainly distributed at the site where nucleus and GFAP-immunopositive structures are in contact (arrowheads). (d) GFAP- and M1R-immunopositive glia limitans (white arrows) lying immediately below the pia mater is observed. The pia mater (magenta arrows) shows slightly weak M1R immunopositivity signals. (e) Enlarged images of framed areas in (d). The glia limitans composed of GFAP-immunopositive surface astrocytes shows "Strong" M1R immunopositivity signals in their somata. Thick processes extending vertically into the cortex are also observed (arrowheads). These images were obtained at 0.8 μm optical thickness. Slice number of image/number of obtained Z-stack optical slices: (a) 2nd/7 slices, (b) 3rd/7 slices, (c) 3rd/6 slices, (d) single slice, (e) 2nd/5 slices. Scale bars = 5 μm in (c) (applies to a–c) and (e), 10 μm in (d)

developmental studies (García-Marqués & López-Mascaraque, 2013; Tabata, 2015). The surface astrocytes were horizontally aligned on the cortical surface and have thick processes extending vertically into the cortex (Tabata, 2015). We found that somata of surface astrocytes show strong M1R immunopositivity signals, as is the case with pyramidal neurons. About 94% of the surface astrocytes showed "Strong–Moderate" of M1R immunopositivity signals. Among them, approximately 83% showed "Strong" signals. The proportion of the surface astrocytes showing "Strong–Moderate" signals was significantly higher than that of the protoplasmic GFAP astrocytes in layer I (Figure 7).

GS immunopositivity signals were found in glia limitans, somata, and thick processes. These structures were the same as those previously observed to be GFAP-immunopositive (Figure 10a, b). Additionally, GS was observed in small peripheral elements, which appear to be thin processes and perisynaptic buds of astrocytes (Figure 10c–e). These observations are generally consistent with previous studies (Robinson, 2001; Kulijewicz-Nawrot et al., 2013). They were often in the close vicinity of M1R-immunopositive spinelike structures that were frequently found along dendritic shafts described above. No M1R immunopositivity signals were detected in these GS-immunopositive small elements.

4 | DISCUSSION

4.1 | M1R in excitatory neurons

This study revealed that most pyramidal neurons in rat PrL showed "Strong–Moderate" signals of M1R immunopositivity. Previous studies have determined the proportion of excitatory neurons containing M1R. For example, by single-cell RT-PCR analysis, M1R mRNA was detected in 61% of layer V pyramidal neurons in the rat visual cortex (Amar, Lucas-Meunier, Baux, & Fossier, 2010). This proportion seems to be substantially lower than that in the present study. On the other hand, in the rat anterior basolateral amygdalar nucleus, all pyramidal neurons were M1R-immunopositive (Muller et al., 2013), as similarly observed in the present study. Furthermore, in macaque monkeys, fewer than 10% of excitatory neurons in V1 and fewer than 40% of those in the secondary visual cortex (V2) showed M1R immunopositivity signals (Disney et al., 2006). These proportions are also significantly lower than that in rat mPFC. The above observations confirm the idea that the proportion of neurons containing M1R is significantly different between cortical regions and animal species (Disney et al., 2006; Disney & Aoki, 2008; Disney & Reynolds, 2014), and it seems likely that M1R in excitatory neurons may be more widely distributed in limbic cortices than in visual cortices. This difference between cortical regions might depend on neuronal activity related to the ascending cholinergic system, because the cholinergic afferent fibers in the rat frontal cortex are denser than that in the occipital and parietal cortices (Mechawar, Cozzari, & Descarries, 2000).

The cholinergic afferent fibers in the rat cortex are distributed in all layers with layers I and V having somewhat higher densities than the other layers (Mechawar et al., 2000). Furthermore, a recent study has demonstrated that synaptic specializations formed by cholinergic

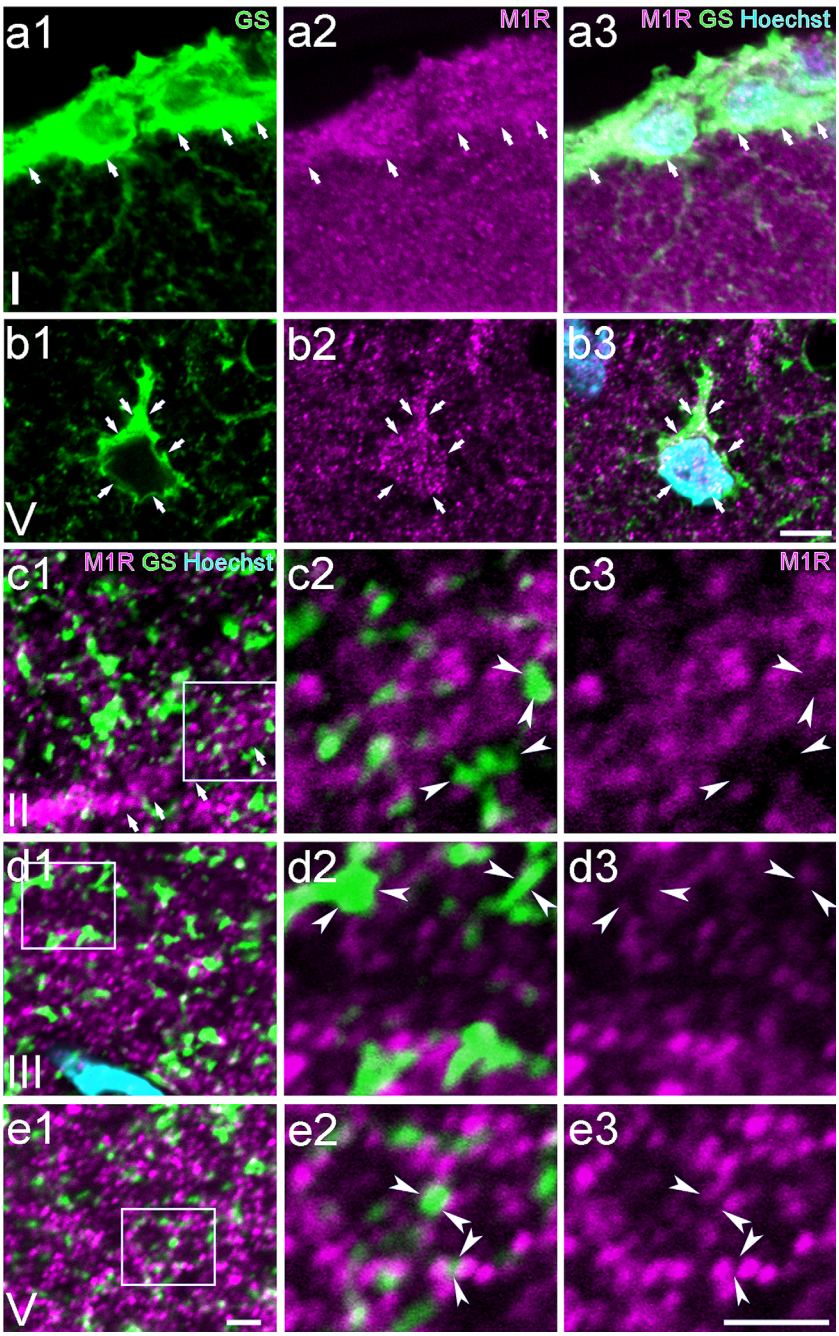

FIGURE 10 M1R immunopositivity signals in GS-immunopositive somata, thin processes, and perisynaptic buds of astrocytes in PrL visualized by confocal laser scanning microscopy showing triple labeling by antibodies to GS (green) and M1R (magenta), and the Hoechst stain (blue). (a) Surface astrocytes in the glia limitans (arrows) show "Strong" M1R immunopositivity signals. (b) GS- and M1R-immunopositive astrocytes are found in all layers. An example in layer V (b) is shown. (c–e) In the neuropils in layers II (c), III (d), and V (e), no M1R immunopositivity signals are detected in the thin processes and perisynaptic buds of astrocytes. Middle and right images are enlarged images of framed areas in (c1–e1). Arrows in (c1) indicate a thick M1R-immunopositive dendrite. On the surface of dendrites as well as in the neuropils, many M1R-immunopositive puncta are distributed. Most of them could be identified as dendritic spines on the basis of their size and uniformly round shape. GS immunopositivity signals are observed in small elements (arrowheads in c–e). They are irregular in shape and appear to be thin processes and perisynaptic buds of astrocytes. They are often in the close vicinity of M1R-immunopositive dendritic spines. No GS-immunopositive small elements showing M1R immunopositivity signals are detected. These images were obtained at 0.8 μm optical thickness. Slice number of image/number of obtained Z-stack optical slices: (a) 2nd/4 slices, (b) 4th/7 slices, (c) 1st/5 slices, (d and e), single slices. Scale bars = 5 μm in (b) (applies to a and b), 2 μm in (e1) (applies to c1–e1), and (e3) (applies to c2–e2, and c3–e3)

varicosities are infrequent, and M1R preferentially localizes on the extrasynaptic membrane of postsynaptic elements (Yamasaki et al., 2010). Moreover, the amount of extracellular acetylcholine in the CA1 area of the hippocampus (hippocampal CA1) significantly increases during learning, and remains high for 60 min (Mitsushima, Sano, & Takahashi, 2013). Therefore, these findings strongly suggest that volume

transmission is the major transmission mechanism in M1R-mediated cholinergic neurotransmission (Sarter, Parikh, & Howe, 2009). From these observations, the cholinergic afferents could widely and diffusely exert their effect on all layers including layers II–V, which contain many pyramidal neurons showing "Strong–Moderate" signals of M1R immunopositivity.

We observed many dendrites and spines showing M1R immunopositivity signals. Dendritic spines are specialized structures where excitatory glutamatergic inputs terminate, and excitatory transmission and synaptic plasticity are modulated (Yao, Spealman, & Zhang, 2008). Pharmacological studies of pyramidal neurons in hippocampal CA1 have demonstrated that muscarinic receptors mediate the increase in intracellular Ca^{2+} concentrations, subsequent activation of CAMKII, and induction of long-term potentiation (LTP) (Müller & Connor, 1991; Müller, Petrozzino, Griffith, Danho, & Connor, 1992; Dennis et al., 2016). Furthermore, both postsynaptic Ca^{2+} concentration elevation and long-lasting enhancement of excitatory postsynaptic currents (EPSCs) are induced by the activation of M1R via IP3 receptors (Fernández de Sevilla, Núñez, Borde, Malinow, & Buño, 2008). Stimulation of M1R also mediates the plasticity of excitatory synapses via insertion of AMPA receptors into postsynaptic sites (Mitsushima et al., 2013). During LTP induced by two-photon glutamate uncaging, CaMKII activation is largely restricted to a stimulated spine. Thus, the CaMKII activity of a stimulated spine has no effect on neighboring spines through dendritic shafts (Lee, Escobedo-Lozoya, Szatmari, & Yasuda, 2009). Thus, M1R modulates signal transduction cascades generated in dendritic spines, and the cascades must play an important role in forming plasticity in each spine.

Acetylcholine application excites cortical pyramidal neurons, for example, prolonged depolarization and increase in spike frequency. Additionally, the initial transient hyperpolarization occurs in layer V pyramidal neurons but not in superficial layer neurons (McCormick, 1992; Gulledge, Park, Kawaguchi, & Stuart, 2007; Gulledge et al., 2009). That is, acetylcholine application elicits different neuronal responses depending on the layer in the rodent neocortex including mPFC. We observed, however, that most pyramidal neurons showed uniformly "Strong–Moderate" signals of M1R immunopositivity. It has been demonstrated that the initial transient hyperpolarization of layer V pyramidal neurons is mediated by small conductance Ca^{2+}-activated K^+ channels (SK channels) via M1R (Gulledge et al., 2007). Moreover, this transient hyperpolarization disappears in pyramidal neurons in M1R-KO mice but not in M3R-KO and M5R-KO mice (Gulledge et al., 2009). The difference in transient hyperpolarization responses between the superficial and deep layers might depend on the expression of signal molecules related to SK channels and/or M1R. Actually, major components of SK channels, SK1 and SK2, are more highly expressed in the pyramidal neurons in layer V than in those in the superficial layers (Stocker & Pedarzani, 2000).

With regard to the prolonged excitation induced by acetylcholine application, a pharmacological study has demonstrated that bath application of carbamylcholine-chloride (CCh), a cholinergic agonist, enhanced cortical neuronal firing. This enhanced firing was antagonized by atropine (M1R–M5R antagonist) and pirenzepine (M1R/M4R antagonist) but not by AF-DX 116 (M2R/M4R antagonist). Thus, it seems likely that the increase in firing frequency induced by CCh is mediated by M1R (Gigout et al., 2012). The increase in the firing frequency of pyramidal neurons induced by CCh via M1R is mimicked by a blocker of Kv7 channels, which are the principal molecular components of M-channels (Brown & Passmore, 2009; Gigout et al., 2012), and M-current, a non-inactivating potassium current, does not respond to a muscarinic agonist in sympathetic neurons in M1R-KO mice (Hamilton et al., 1997). Thus, depression of M-current mediated by M1R could be the mechanism underlying spike acceleration of cortical pyramidal neurons. Since MIR is abundantly localized in somata, it most likely modulates the neuronal activity generated in somata.

4.2 | M1R in GABAergic interneurons

This study demonstrated that most GAD67 neurons showed M1R immunopositivity signals. The strength of these signals, however, varied among neurons. In GAD67 neurons, about 44% of neuronal somata showed "Strong–Moderate" signals, and roughly the same number of somata showed "Weak" signals of M1R immunopositivity. This distribution pattern is quite different from that of the pyramidal neurons described above. Cortical GABAergic interneurons are classified into some distinct neuronal subgroups on the basis of their various markers. Among them, PV neurons are the most numerous. In the rat frontal cortex, they account for 43% of the GABAergic interneurons in layer II/III, 61% in layer V, and 51% in layer VI (Kubota et al., 1994). This study demonstrated that the signal strength of M1R immunopositivity also varied among PV neurons. About 61% of PV neurons showed "Strong–Moderate" signals, whereas 31% showed "Weak" signals of M1R immunopositivity. Thus, approximately 90% of both GAD67 neurons and PV neurons showed M1R immunopositivity signals. However, the proportion of these neurons showing "Strong–Moderate" signals of M1R immunopositivity among PV neurons (total percentage: approximately 61%) was somewhat higher than that among GAD67 neurons (total percentage: approximately 44%). A significant difference was observed in layers III and VI (Figure 7). This tendency is in agreement with previous studies on V1 of macaque monkeys, which revealed that M1R was observed in 87% of PV neurons and in 61% of GABAergic neurons (Disney et al., 2006; Disney & Aoki, 2008). Thus, M1R seems to be more preferentially distributed in PV neurons than in other GABAergic neuronal subgroups. Since the signal strength of M1R immunopositivity varied among GAD67 neurons and PV neurons, it might depend on the activity of each neuron induced by cholinergic afferents.

Cortical PV neurons are electrophysiologically classified as fast-spiking neurons, which include basket cells, chandelier cells, and wide arbor cells (Kawaguchi & Kondo, 2002; Hardwick, French, Southam, & Totterdell, 2005). The fast-spiking neurons are characterized by non-adaptive firing of short-duration spikes, and they primarily innervate the somata and initial segments of pyramidal neurons. Thus, they are the most prominent intracortical elements that inhibit excitatory pyramidal neurons. Cea-del Rio et al. (2010) have revealed by single-cell RT-PCR analysis that M1R mRNA was expressed in all PV basket

cells in mouse hippocampal CA1. However, M3R and M5R were not detected in these cells. Hence, M1R is the only M1R-type receptor expressed in PV basket cells. Their finding is in close agreement with our present immunohistochemical data showing that M1R was expressed in over 90% of PV neurons. However, in rat V1 and primary somatosensory cortices, the proportion of somata showing M1R immunopositivity signals among PV neurons were 27% and 21%, respectively (Disney & Reynolds, 2014). These values are significant lower than that in PrL. It is unclear which factors cause this difference. It may be caused by our criterion that somata showing weak signals were counted. There may be other factors as well. Because the present study revealed that the signal intensity of M1R immunopositivity in PV neurons varied from being strong to being negative, several factors, such as differences in neuronal activity, cortical areas, and animal age, might also affect the expression level of M1R in somata.

Yi et al. (2014) have demonstrated the significant increase in firing frequency induced by muscarine in both hippocampal CA1 and PFC PV neurons. Additionally, they observed reduction in both firing frequency and postdepolarization potential in hippocampal CA1 PV neurons of mice with transgenically deleted M1R from PV neurons (PV-M1R-KO mice). This finding is in agreement with the previous finding that muscarine-induced firing acceleration was completely absent in PV basket cells of M1R-KO mice (Cea-del Rio et al., 2010). Because PV-M1R-KO mice are exclusively deficit in recognition and working memory but not in spatial memory, muscarine-induced increase in PV neuronal activity via M1R should be essential in these higher cognitive functions (Yi et al., 2014).

4.3 | M1R in astrocytes

In this study, about 78% of protoplasmic GFAP astrocytes showed "Strong–Moderate" signals, and approximately 12% showed "Weak" signals of M1R immunopositivity. Thus, approximately 90% of astrocytes possess M1R immunopositivity signals. A pharmacological study has demonstrated that cultured astrocytes in the rat cerebral cortex contain both M1-type and M2-type muscarinic receptors (Murphy, Pearce, & Morrow, 1986). Previous studies using a monoclonal antibody to pan-muscarinic receptors also revealed that muscarinic receptors were found in astrocytes in explant and primary cultures derived from the rat cerebral cortex (Hösli, Jurasin, Ruhl, Luthy, & Hösli, 2001), and in almost all (95.8%) of GFAP astrocytes in the rat frontal cortex (van der Zee, de Jong, Strosberg, & Luiten, 1993). Furthermore, in human cultured astrocytes, all five subtypes of muscarinic receptors were detected by RT-PCR analysis (Elhusseiny et al., 1999), and pharmacological analysis has revealed that astrocytes in rat hippocampal slices possess M1R (Shelton & McCarthy, 2000).

The present study also revealed that M1R immunopositivity signals were preferentially localized in astrocytic somata, and they were hardly detected in thin processes and perisynaptic buds. In the gray matter, the protoplasmic astrocytes play important roles in various functions that support the structural, trophic, and metabolic properties of neurons (Chen & Swanson, 2003; Sofroniew & Vinters, 2010). Furthermore, astrocytes also contibute to the modulation of excitatory synaptic transmission by releasing gliotransmitters, such as glutamate, ATP, and D-serine, which is an NMDA receptor coagonist (Agulhon et al., 2008; Takata et al., 2011;Agulhon et al., 2012). Recently, it has been demonstrated that each astrocyte forms a domain composed of its soma and processes containing perisynaptic buds (Khakh & McCarthy, 2015). Interestingly, each domain only slightly overlaps with other domains (Wilhelmsson et al., 2006). It has been estimated that a domain is 66,000 μm^3 in size and contains ~140,000 synapses in hippocampal CA1 (Bushong, Martone, Jones, & Ellisman, 2002). Thus, over 100,000 synapses are modulated by a single astrocyte. Furthermore, because astrocytes link to other astrocytes via gap junctions, activation of an astrocyte might exert its influence over a wider extent (Kimelberg, 2010).

Takata et al. (2011) have observed that stimulation of BF increased the whisker-evoked local field potential in the mouse barrel cortex. During the enhancement of local field potential, the increase in astrocytic Ca^{2+} concentration is followed by a significant increase in the extracellular concentration of D-serine. The increase in astrocytic Ca^{2+} concentration was blocked by atropine, a muscarinic receptor antagonist. Similarly, the increase in astrocytic Ca^{2+} concentration and the following release of D-serine are diminished in inositol-1,4,5-triphosphate receptor type 2-KO (IP_3R2-KO) mice. Thus, the release of D-serine is triggered by the increase in astrocytic Ca^{2+} concentration via IP_3R2 (Agulhon et al., 2012). Another pharmacological study has revealed that a cholinergic receptor agonist, carbachol, induces an increase in astrocytic Ca^{2+} concentration, and this increase is blocked by pirenzepine (M1R/M4R antagonist) (Shelton & McCarthy, 2000). Since M1-type receptors but not M2-type receptors preferentially stimulate PLC, which in turn stimulates IP_3R2, the acetylcholine-induced increase in astrocytic Ca^{2+} concentration and the following release of D-serine are mediated by both M1R and IP_3R2. However, synaptic transmission events need a timescale of milliseconds, whereas, gliotransmission events need a timescale of seconds. Thus, it is quite plausible that gliotransmission via astrocytic processes is not possible for modulation of each synaptic transmission (Agulhon et al., 2012). Additionally, since M1R is mainly localized in astrocytic somata but hardly detected in perisynaptic buds and thin processes, it is seems likely that synaptic transmissions are widely modulated in a group by each astrocytic domain and/or domains linked by gap junctions.

This idea is confirmed by a recent electrophysiological study (Letellier et al., 2016). This study revealed that changes in the presynaptic strength of synapses that receive inputs from a certain neuron induce alterations in presynaptic strengths of neighboring synapses that receive no inputs from that neuron. Because this interaction between synapses is inhibited by fluoroacetate, an inhibitor of the Krebs cycle that preferentially acts on glial cells, a synapse can exert its effect on the presynaptic strengths of other synapses via astrocytes.

The glia limitans lying immediately below the pia mater is composed of end-feet of astrocytes in humans and primates, as described in any histology textbook. In rodents, however, it is composed of surface astrocytes that exhibit a fibroblast-like morphology (García-Marqués & López-Mascaraque, 2013; Liu et al., 2013; Tabata, 2015). The present study revealed that many surface astrocytes show "Strong"

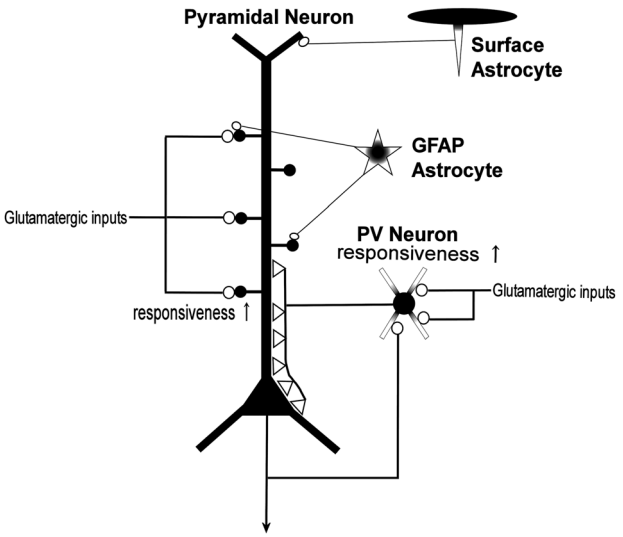

FIGURE 11 Hypothetical schematic diagram illustrating neuronal circuit between pyramidal neurons, PV neurons, and astrocytes. In pyramidal neurons, M1R is widely distributed in somata, dendritic shafts, and spines (black). In PV neurons, M1R is preferentially distributed in somata (black), whereas it is sparsely distributed in dendrites (gray to white). No M1R is detected in axon terminals (open circles and open triangles). Electrophysiological studies (see text) demonstrated that the combination of activation of M1R and glutamatergic inputs (open circles) induces LTP in dendritic spines of pyramidal neurons and increases the firing frequency of both pyramidal neurons and PV neurons that strongly inhibit (open triangles) the activity of pyramidal neurons. Activation of M1R in both excitatory pyramidal neurons and inhibitory PV neurons may underlie the generation of gamma oscillation, which plays an important role in the control of propagation of cortical information. M1R is also found in the somata of GFAP astrocytes and surface astrocytes, but it is not detected in their processes and perisynaptic buds (open ellipses). Astrocytic M1R may modulate glutamatergic synaptic transmission at synaptic sites in a group by each astrocytic domain (see text), and modulate the firing mode of pyramidal neurons at dendritic tufts in layer I

signals of M1R immunopositivity, and frequently have thick processes projecting toward layer I of the cerebral cortex, which is composed of axon fibers and tufts originating from apical dendrites of pyramidal neurons. This layer is crucial in the control of the firing mode of pyramidal neurons via apical dendritic calcium channels. Activation of these channels increases neuronal gain and switches the mode of these neurons to burst firing (Sidiropoulou, Pissadaki, & Poirazi, 2006; Murayama et al., 2009). Surface astrocytes might modulate synaptic activities in layer I and control the firing mode of pyramidal neurons through cholinergic afferents via M1R.

4.4 | Functional implications

This study revealed that almost all PV neuronal somata expressed M1R. However, M1R was not detected in their thin distal dendrites. Thus, the intracellular localization pattern of M1R in PV neurons was quite different from that of pyramidal neurons in which M1R was widely expressed in somata, dendrites, and spines (Figure 11). Interestingly, these intracellular distribution patterns of M1R in pyramidal neurons and PV neurons are quite similar to those of dopamine receptor D5 (D5R) in rat PrL.

Dopamine is a notable neuromodulator similarly to acetylcholine. D1-type receptors (D1R and D5R) of dopamine are metabolic receptors, and they enhance the responsiveness of both pyramidal neurons and PV neurons via signal transduction cascades including the activation of adenyl cyclase and the increase in the concentrations of cAMP and protein kinase A (Trantham-Davidson, Neely, Lavin, & Seamans, 2004; Kröner, Krimer, Lewis, & Barrionuevo, 2007; Thurley, Senn, & Lüscher, 2008). In the rodent cerebral cortex, D5R is the predominant D1-type receptor (Luedtke et al., 1999). As in the case of M1R, D5R was found in somata, proximal and distal dendrites as well as in dendritic spines in pyramidal neurons. On the other hand, D5R was restricted in somata and proximal dendrites in PV neurons (Oda et al., 2010). Since M1R and D5R activate different signal transduction cascades, the cascade activated by M1R and that by D5R might interfere with each other in areas where they colocalize, such as somata, dendrites, and dendritic spines.

Additionally, a similar intracellular distribution pattern was also observed in the thalamus. M3R is the predominant M1-type receptor in the thalamus. In the anteroventral (AV) and anterodorsal (AD) thalamic nuclei, M3R is distributed throughout the dendrites and somata of excitatory relay neurons (Oda, Kuroda, Kakuta, & Kishi, 2001). On the other hand, it is distributed chiefly in the somata and proximal dendrites in PV neurons of the reticular thalamic nucleus, which sends inhibitory projections to relay neurons in AV and AD (Oda et al., 2007). Neuromodulators widely and diffusely exert their effects on both excitatory and inhibitory neurons via volume transmission. The intracellular distribution patterns of their receptors are, however, quite different between excitatory and PV neurons.

These observations strongly suggest that the modulators exert their effects on each neuronal type via intracellular signaling cascades located in neuronal domains where the receptors are expressed. Therefore, acetylcholine might exert its effect via M1R on somata, throughout dendritic shafts as well as dendritic spines in pyramidal neurons, whereas it preferentially exerts its effect via M1R on the somata of inhibitory neurons. That is, M1R may mediate neuronal activity such as firing acceleration in the somata of both excitatory and inhibitory neurons. Furthermore, M1R may mediate the induction of LTP in dendritic spines and the control of neuronal activity modes in tufts of apical dendrites derived from pyramidal neurons.

PV neurons have reciprocal fiber connections with excitatory pyramidal neurons. Activated M1R increases the activity of both excitatory and inhibitory PV neurons. Thus, a question arises. How are the intracortical circuits between excitatory and PV neurons modulated by M1R?

Recently, it has been suggested that the reciprocal connections between excitatory pyramidal neurons and inhibitory PV neurons play an important role in the generation of cortical gamma oscillation (Brown, Basheer, McKenna, Strecker, & McCarley, 2012), which is called the pyramidal interneuron network gamma (PING) model. Gamma (20–80 Hz) frequency rhythms are a prominent feature of

electroencephalograms during awakening and gamma frequency increases during focused attention (Cardin et al., 2009). Because PV neurons connect with each other using electrical synapses via gap junctions, synchronously rhythmic inhibition and disinhibition occur in the perisomatic region of pyramidal neurons (Galarreta & Hestrin, 1999; Hestrin & Galarreta, 2005; Fukuda, Kosaka, Singer, & Galuske, 2006). Electrophysiological studies have revealed that both the cholinergic agonist carbacol and the nonselective muscarinic receptor agonist muscarine induce gamma oscillation in the hippocampus and PFC in vitro (Fisahn, Pike, Buhl, & Paulsen, 1998; Fellous & Sejnowski, 2000; Pafundo, Miyamae, Lewis, & Gonzalez-Burgos, 2013). Furthermore, in M1R-KO mice, muscarine fails to induce gamma oscillation (Fisahn et al., 2002). Therefore, activation of M1R in both excitatory pyramidal neurons and inhibitory PV neurons may most likely underlie the generation of gamma oscillation. Moreover, because the timing of inputs relative to a gamma cycle determines the amplitude and accuracy of evoked responses, gamma oscillation plays an important role in the control of intracortical transmission (Cardin et al., 2009). Therefore, the mechanism of M1R-induced gamma oscillation in PFC should be an essential element for processing cognitive functions.

Since the cholinergic innervation of the cortex is considerably diffuse and cholinergic transmission is mediated by volume transmission in the extrasynaptic space (Sarter et al., 2009), the cholinergic system may exert its influence over a wide range of neural elements, such as excitatory neurons, inhibitory neurons, and astrocytes. The differential intracellular localization of M1R in these cells might play a crucial role in the transmission of information and the plasticity of spines, and underlie the cognitive functions subserved by PrL.

CONFLICT OF INTEREST

The authors have no conflicts of interest.

AUTHOR CONTRIBUTIONS

All authors had full access to all the data in the study and take responsibility for the integrity of the data and the accuracy of data analysis. Study concept and design: SO, HF. Acquisition of data: SO, YT, MI. Analysis and interpretation of data: SO, SA-A. Drafting of the manuscript: SO, HF, MK. Critical revision of the manuscript for important intellectual content: SO, HF. Statistical analysis: SO, SY. Obtained funding: SO, HF, YT. Administrative, technical, and material support: SO, SY, MI. Study supervision: SO.

ORCID

Satoko Oda http://orcid.org/0000-0001-7248-5957
Hiromasa Funato http://orcid.org/0000-0002-2787-9700

REFERENCES

Agulhon, C., Petravicz, J., McMullen, A. B., Sweger, E. J., Minton, S. K., Taves, S. R., … McCarthy, K. D. (2008). What is the role of astrocyte calcium in neurophysiology?. *Neuron*, *59*(6), 932–946.

Agulhon, C., Sun, M. Y., Murphy, T., Myers, T., Lauderdale, K., & Fiacco, T. A. (2012). Calcium signaling and gliotransmission in normal vs. reactive astrocytes. *Frontiers in Pharmacology*, *3*(139), 1–16.

Allen Institute for Brain Science. (2004). *Allen mouse brain atlas*. Retrieved from: http://mouse.brain-map.org/

Amar, M., Lucas-Meunier, E., Baux, G., & Fossier, P. (2010). Blockade of different muscarinic receptor subtypes changes the equilibrium between excitation and inhibition in rat visual cortex. *Neuroscience*, *169*(4), 1610–1620.

Bellocchio, E. E., Hu, H., Pohorille, A., Chan, J., Pickel, V. M., & Edwards, R. H. (1998). The localization of the brain-specific inorganic phosphate transporter suggests a specific presynaptic role in glutamatergic transmission. *Journal of Neuroscience*, *18*(21), 8648–8659.

Birrell, J. M., & Brown, V. J. (2000). Medial frontal cortex mediates perceptual attentional set shifting in the rat. *Journal of Neuroscience*, *20*(11), 4320–4324.

Brown, D. A., & Passmore, G. M. (2009). Neural KCNQ (Kv7) channels. *British Journal of Pharmacology*, *156*(8), 1185–1195.

Brown, R. E., Basheer, R., McKenna, J. T., Strecker, R. E., & McCarley, R. W. (2012). Control of sleep and wakefulness. *Physiological Reviews*, *92*(3), 1087–1187.

Browne, S. E., Lin, L., Mattsson, A., Georgievska, B., & Isacson, O. (2001). Selective antibody-induced cholinergic cell and synapse loss produce sustained hippocampal and cortical hypometabolism with correlated cognitive deficits. *Experimental Neurology*, *170*(1), 36–47.

Buckman, L. B., Thompson, M. M., Moreno, H. N., & Ellacott, K. L. J. (2013). Regional astrogliosis in the mouse hypothalamus in response to obesity. *Journal of Comparative Neurology*, *521*(6), 1322–1333.

Burette, A. C., Strehler, E. E., & Weinberg, R. J. (2009). Fast" plasma membrane calcium pump PMCA2a concentrates in GABAergic terminals in the adult rat brain. *Journal of Comparative Neurology*, *512*(4), 500–513.

Bushong, E. A., Martone, M. E., Jones, Y. Z., & Ellisman, M. H. (2002). Protoplasmic astrocytes in CA1 stratum radiatum occupy separate anatomical domains. *The Journal of Neuroscience* , *22*(1), 183–192.

Carballo-Márquez, A., Vale-Martínez, A., Guillazo-Blanch, G., Torras-Garcia, M., Boix-Trelis, N., & Martí-Nicolovius, M. (2007). Differential effects of muscarinic receptor blockade in prelimbic cortex on acquisition and memory formation of an odor-reward task. *Learning & Memory*, *14*(9), 616–624.

Cardin, J. A., Carlén, M., Meletis, K., Knoblich, U., Zhang, F., Deisseroth, K., … Moore, C. I. (2009). Driving fast-spiking cells induces gamma rhythm and controls sensory responses. *Nature*, *459*(7247), 663–667.

Cea-del Rio, C. A., Lawrence, J. J., Tricoire, L., Erdelyi, F., Szabo, G., & McBain, C. J. (2010). M3 muscarinic acetylcholine receptor expression confers differential cholinergic modulation to neurochemically distinct hippocampal basket cell subtypes. *Journal of Neuroscience*, *30*(17), 6011–6024.

Chang, M. L., Wu, C. H., Jiang-Shieh, Y. F., Shieh, J. Y., & Wen, C. Y. (2007). Reactive changes of retinal astrocytes and Müller glial cells in kainate-induced neuroexcitotoxicity. *Journal of Anatomy*, *210*(1), 54–65.

Chen, N., Sugihara, H., Sharma, J., Perea, G., Petravicz, J., Le, C., & Sur, M. (2012). Nucleus basalis-enabled stimulus-specific plasticity in the visual cortex is mediated by astrocytes. *Proceedings of the National Academy of Sciences of the United States of America*, *109*(41), E2832–E2841.

Chen, Y., & Swanson, R. A. (2003). Astrocytes and brain injury. *Journal of Cerebral Blood Flow and Metabolism*, *23*(2), 137–149.

de Bruin, J. P. C., Moita, M. P., de Brabander, H. M., & Joosten, R. N. J. M. A. (2001). Place and response learning of rats in a Morris Water

Maze: Differential effects of Fimbria fornix and medial prefrontal cortex lesions. *Neurobiology of Learning and Memory*, *75*(2), 164–178.

Dehmelt, L., & Halpain, S. (2004). The MAP2/Tau family of microtubule-associated proteins. *Genome Biology*, *6*(1), 204.

Dennis, S. H., Pasqui, F., Colvin, E. M., Sanger, H., Mogg, A. J., Felder, C. C., … Mellor, J. R. (2016). Activation of muscarinic M1 acetylcholine receptors induces long-term potentiation in the hippocampus. *Cerebral Cortex*, *26*(1), 414–426.

Disney, A. A., & Aoki, C. (2008). Muscarinic acetylcholine receptors in macaque V1 are most frequently expressed by parvalbumin-immunoreactive neurons. *Journal of Comparative Neurology*, *507*(5), 1748–1762.

Disney, A. A., Domakonda, K. V., & Aoki, C. (2006). Differential expression of muscarinic acetylcholine receptors across excitatory and inhibitory cells in visual cortical areas V1 and V2 of the macaque monkey. *The Journal of Comparative Neurology*, *499*(1), 49–63.

Disney, A. A., & Reynolds, J. H. (2014). Expression of m1-type muscarinic acetylcholine receptors by parvalbumin-immunoreactive neurons in the primary visual cortex: A comparative study of rat, guinea pig, ferret, macaque, and human. *Journal of Comparative Neurology*, *522*(5), 986–1003.

Eglen, R. M. (2012). Overview of muscarinic receptor subtypes. *Handbook of Experimental Pharmacology*, *208*, 3–28.

Elhusseiny, A., Cohen, Z., Olivier, A., Stanimirović, D. B., & Hamel, E. (1999). Functional acetylcholine muscarinic receptor subtypes in human brain microcirculation: Identification and cellular localization. *Journal of Cerebral Blood Flow and Metabolism*, *19*(7), 794–802.

Ethier, K., Rompré, P., & Godbout, R. (2001). Spatial strategy elaboration in egocentric and allocentric tasks following medial prefrontal cortex lesions in the rat. *Brain and Cognition*, *46*(1), 134–135.

Felder, C. C., Porter, A. C., Skillman, T. L., Zhang, L., Bymaster, F. P., Nathanson, N. M., … McKinzie, D. L. (2001). Elucidating the role of muscarinic receptors in psychosis. *Life Sciences*, *68*(22–23), 2605–2613.

Fellous, J. M., & Sejnowski, T. J. (2000). Cholinergic induction of oscillations in the hippocampal slice in the slow (0.5-2 Hz), theta (5–12 Hz), and gamma (35–70 Hz) bands. *Hippocampus*, *10*(2), 187–197.

Fernández de Sevilla, D., Núñez, A., Borde, M., Malinow, R., & Buño, W. (2008). Cholinergic-mediated IP3-receptor activation induces long-lasting synaptic enhancement in CA1 pyramidal neurons. *The Journal of Neuroscience*, *28*(6), 1469–1478.

Fisahn, A., Pike, F. G., Buhl, E. H., & Paulsen, O. (1998). Cholinergic induction of network oscillations at 40 Hz in the hippocampus in vitro. *Nature*, *394*(6689), 186–189.

Fisahn, A., Yamada, M., Duttaroy, A., Gan, J. W., Deng, C. X., McBain, C. J., & Wess, J. (2002). Muscarinic induction of hippocampal gamma oscillations requires coupling of the M1 receptor to two mixed cation currents. *Neuron*, *33*(4), 615–624.

Fuentes-Santamaría, V., Alvarado, J. C., Gabaldón-Ull, M. C., & Manuel Juiz, J. (2013). Upregulation of insulin-like growth factor and interleukin 1β occurs in neurons but not in glial cells in the cochlear nucleus following cochlear ablation. *Journal of Comparative Neurology*, *521*(15), 3478–3499.

Fujiyama, F., Furuta, T., & Kaneko, T. (2001). Immunocytochemical localization of candidates for vesicular glutamate transporters in the rat cerebral cortex. *Journal of Comparative Neurology*, *435(February)*, 379–387.,

Fukuda, T., Kosaka, T., Singer, W., & Galuske, R. A. W. (2006). Gap junctions among dendrites of cortical GABAergic neurons establish a dense and widespread intercolumnar network. *Journal of Neuroscience*, *26*(13), 3434–3443.

Galarreta, M., & Hestrin, S. (1999). A network of fast-spiking cells in the neocortex connected by electrical synapses. *Nature*, *402*(6757), 72–75.

García-Marqués, J., & López-Mascaraque, L. (2013). Clonal identity determines astrocyte cortical heterogeneity. *Cerebral Cortex*, *23*(6), 1463–1472.

Gigout, S., Jones, G. A., Wierschke, S., Davies, C. H., Watson, J. M., & Deisz, R. A. (2012). Distinct muscarinic acetylcholine receptor subtypes mediate pre- and postsynaptic effects in rat neocortex. *BMC Neuroscience*, *13*(1), 1–14.

Grothe, M. J., Heinsen, H., Amaro, E., Grinberg, L. T., & Teipel, S. J. (2016). Cognitive correlates of basal forebrain atrophy and associated cortical hypometabolism in mild cognitive impairment. *Cerebral Cortex*, *26*(6), 2411–2426.

Gulledge, A. T., Bucci, D. J., Zhang, S. S., Matsui, M., & Yeh, H. H. (2009). M1 receptors mediate cholinergic modulation of excitability in neocortical pyramidal neurons. *Journal of Neuroscience*, *29*(31), 9888–9902.

Gulledge, A. T., Park, S. B., Kawaguchi, Y., & Stuart, G. J. (2007). Heterogeneity of phasic cholinergic signaling in neocortical neurons. *Journal of Neurophysiology*, *97*(3), 2215–2229.

Hamilton, S. E., Loose, M. D., Qi, M., Levey, A. I., Hille, B., McKnight, G. S., … Nathanson, N. M. (1997). Disruption of the m1 receptor gene ablates muscarinic receptor-dependent M current regulation and seizure activity in mice. *Proceedings of the National Academy of Sciences of the United States of America*, *94*(24), 13311–13316.

Hardwick, C., French, S. J., Southam, E., & Totterdell, S. (2005). A comparison of possible markers for chandelier cartridges in rat medial prefrontal cortex and hippocampus. *Brain Research*, *1031*(2), 238–244.

Hestrin, S., & Galarreta, M. (2005). Electrical synapses define networks of neocortical GABAergic neurons. *Trends in Neurosciences*, *28*(6 SPEC. ISS), 304–309.

Hösli, E., Jurasin, K., Ruhl, W., Luthy, R., & Hösli, L. (2001). Colocalization of androgen, estrogen and cholinergic receptors on cultured astrocytes of rat central nervous system. *International Journal of Developmental Neuroscience*, *19*(1), 11–19.

Jabs, R., Paterson, I. A., & Walz, W. (1997). Qualitative analysis of membrane currents in glial cells from normal and gliotic tissue in situ: Down-regulation of Na+ current and lack of P2 purinergic responses. *Neuroscience*, *81*(3), 847–860.

Johnson, R. T., Breedlove, S. M., & Jordan, C. L. (2013). Androgen receptors mediate masculinization of astrocytes in the rat posterodorsal medial amygdala during puberty. *Journal of Comparative Neurology*, *521*(10), 2298–2309.

Kadriu, B., Guidotti, A., Chen, Y., & Grayson, D. R. (2012). DNA methyltransferases1 (DNMT1) and 3a (DNMT3a) colocalize with GAD67-positive neurons in the GAD67-GFP mouse brain. *The Journal of Comparative Neurology*, *520*(9), 1951–1964.

Kaneko, T., Fujiyama, F., & Hioki, H. (2002). Immunohistochemical localization of candidates for vesicular glutamate transporters in the rat brain. *Journal of Comparative Neurology*, *444*(1), 39–62.

Kaufman, D. L., Houser, C. R., & Tobin, A. J. (1991). Two forms of the gamma-aminobutyric acid synthetic enzyme glutamate decarboxylase have distinct intraneuronal distributions and cofactor interactions. *Journal of Neurochemistry*, *56*(2), 720–723.

Kawaguchi, Y., & Kondo, S. (2002). Parvalbumin, somatostatin and cholecystokinin as chemical markers for specific GABAergic interneuron types in the rat frontal cortex. *Journal of Neurocytology*, *31(3–5 SPEC)*, 277–287.

Keil, A. (2004). The role of human prefrontal cortex in motivated perception and behavior: A macroscopic perspective. In S. Otani (Ed.), *Prefrontal cortex: from synaptic plasticity to cognition* (pp. 245–268). Boston, MA: Kluwer Academic Publishers.

Khakh, B. S., & McCarthy, K. D. (2015). Astrocyte calcium signaling: From observations to functions and the challenges therein. *Cold Spring Harbor Perspectives in Biology*, *7*(4), a020404.

Kimelberg, H. K. (2009). Chapter 1. Astrocyte heterogeneity or homogeneity?. In V. Parpura &, P. G. Haydon (Eds.), *Astrocytes in (patho) physiology of the nervous system* (pp. 1–25). Philadelphia, NY: Springer.

Kimelberg, H. K. (2010). Functions of mature mammalian astrocytes: A current view. *The Neuroscientist*, *16*(1), 79–106.

Kristensen, B. W., Noer, H., Gramsbergen, J. B., Zimmer, J., & Noraberg, J. (2003). Colchicine induces apoptosis in organotypic hippocampal slice cultures. *Brain Research*, *964*(2), 264–278.

Kröner, S., Krimer, L. S., Lewis, D. A., & Barrionuevo, G. (2007). Dopamine increases inhibition in the monkey dorsolateral prefrontal cortex through cell type-specific modulation of interneurons. *Cerebral Cortex*, *17*(5), 1020–1032.

Kubota, Y., Hattori, R., & Yui, Y. (1994). Three distinct subpopulations of GABAergic neurons in rat frontal agranular cortex. *Brain Research*, *649*(1–2), 159–173.

Kulijewicz-Nawrot, M., Syková, E., Chvátal, A., Verkhratsky, A., & Rodríguez, J. J. (2013). Astrocytes and glutamate homoeostasis in Alzheimer's disease: A decrease in glutamine synthetase, but not in glutamate transporter-1, in the prefrontal cortex. *ASN Neuro*, *5*(4), 273–282.

Lee, J. E., Jeong, D. U., Lee, J., Chang, W. S., & Chang, J. W. (2016). The effect of nucleus basalis magnocellularis deep brain stimulation on memory function in a rat model of dementia. *BMC Neurology*, *16*(1), 6.

Lee, S.-J. R., Escobedo-Lozoya, Y., Szatmari, E. M., & Yasuda, R. (2009). Activation of CaMKII in single dendritic spines during long-term potentiation. *Nature*, *458*(7236), 299–304.

Letellier, M., Park, Y. K., Chater, T. E., Chipman, P. H., Gautam, S. G., Oshima-Takago, T., & Goda, Y. (2016). Astrocytes regulate heterogeneity of presynaptic strengths in hippocampal networks. *Proceedings of the National Academy of Sciences of the United States of America*, *113*(19), E2685–E2694.

Levey, A. I., Kitt, C. A., Simonds, W. F., Price, D. L., & Brann, M. R. (1991). Identification and localization of muscarinic acetylcholine receptor proteins in brain with subtype-specific antibodies. *The Journal of Neuroscience*, *11*(10), 3218–3226.

Ling, E. A., & Leblond, C. P. (1973). Investigation of glial cells in semithin sections. II. Variation with age in the numbers of the various glial cell types in rat cortex and corpus callosum. *Journal of Comparative Neurology*, *149*(1), 73–82.

Ling, E. A., Paterson, J. A., Privat, A., Mori, S., & Leblond, C. P. (1973). Investigation of glial cells in semithin sections. I. Identification of glial cells in the brain of young rats. *Journal of Comparative Neurology*, *149*(1), 43–71.

Liu, X., Zhang, Z., Guo, W., Burnstock, G., He, C., & Xiang, Z. (2013). The superficial glia limitans of mouse and monkey brain and spinal cord. *Anatomical Record (Hoboken, N.J.:2007)*, *296*(7), 995–1007.

Lucas-Meunier, E., Fossier, P., Baux, G., & Amar, M. (2003). Cholinergic modulation of the cortical neuronal network. *Pflügers Archiv - European Journal of Physiology*, *446*(1), 17–29.

Luedtke, R. R., Griffin, S. A., Conroy, S. S., Jin, X., Pinto, A., & Sesack, S. R. (1999). Immunoblot and immunohistochemical comparison of murine monoclonal antibodies specific for the rat D1a and D1b dopamine receptor subtypes. *Journal of Neuroimmunology*, *101*(2), 170–187.

Matsunaga, W., Miyata, S., Hashimoto, Y., Lin, S. H., Nakashima, T., Kiyohara, T., & Matsumoto, T. (1999). Microtubule-associated protein-2 in the hypothalamo-neurohypophysial system: Low-molecular-weight microtubule-associated protein-2 in pituitary astrocytes. *Neuroscience*, *88*(4), 1289–1297.

McCormick, D. A. (1992). Neurotransmitter actions in the thalamus and cerebral cortex and their role in neuromodulation of thalamocortical activity. *Progress in Neurobiology*, *39*(4), 337–388.

Mechawar, N., Cozzari, C., & Descarries, L. (2000). Cholinergic innervation in adult rat cerebral cortex: A quantitative immunocytochemical description. *Journal of Comparative Neurology*, *428*(2), 305–318.

Melone, M., Burette, A., & Weinberg, R. J. (2005). Light microscopic identification and immunocytochemical characterization of glutamatergic synapses in brain sections. *Journal of Comparative Neurology*, *492*(4), 495–509.

Middeldorp, J., & Hol, E. M. (2011). GFAP in health and disease. *Progress in Neurobiology*, *93*(3), 421–443.

Mitsushima, D., Sano, A., & Takahashi, T. (2013). A cholinergic trigger drives learning-induced plasticity at hippocampal synapses. *Nature Communications*, *4*, 2760.

Mrzljak, L., Levey, A. I., & Goldman-Rakic, P. S. (1993). Association of m1 and m2 muscarinic receptor proteins with asymmetric synapses in the primate cerebral cortex: Morphological evidence for cholinergic modulation of excitatory neurotransmission. *Proceedings of the National Academy of Sciences of the United States of America*, *90*(11), 5194–5198.

Muller, J. F., Mascagni, F., Zaric, V., & Mcdonald, A. J. (2013). Muscarinic cholinergic receptor M1 in the rat basolateral amygdala: Ultrastructural localization and synaptic relationships to cholinergic axons. *Journal of Comparative Neurology*, *521*(8), 1743–1759.

Müller, W., & Connor, J. A. (1991). Cholinergic input uncouples Ca2+ changes from K+ conductance activation and amplifies intradendritic Ca2+ changes in hippocampal neurons. *Neuron*, *6*(6), 901–905.

Müller, W., Petrozzino, J. J., Griffith, L. C., Danho, W., & Connor, J. A. (1992). Specific involvement of Ca-2+ calmodulin kinase-II in cholinergic modulation of neuronal responsiveness. *Journal of Neurophysiology*, *68*(6), 2264–2269.

Murayama, M., Pérez-Garci, E., Nevian, T., Bock, T., Senn, W., & Larkum, M. E. (2009). Dendritic encoding of sensory stimuli controlled by deep cortical interneurons. *Nature*, *457*(7233), 1137–1141.

Murphy, S., Pearce, B., & Morrow, C. (1986). Astrocytes have both M1 and M2 muscarinic receptor subtypes. *Brain Research*, *364*(1), 177–180.

Nasonkin, I. O., Lazo, K., Hambright, D., Brooks, M., Fariss, R., & Swaroop, A. (2011). Distinct nuclear localization patterns of DNA methyltransferases in developing and mature mammalian retina. *The Journal of Comparative Neurology*, *519*(10), 1914–1930.

Nichols, N. R., Day, J. R., Laping, N. J., Johnson, S. A., & Finch, C. E. (1993). GFAP mRNA increases with age in rat and human brain. *Neurobiology of Aging*, *14*(5), 421–429.

Norenberg, M. D., & Martinez-Hernandez, A. (1979). Fine structural localization of glutamine synthetase in astrocytes of rat brain. *Brain Research*, *161*(2), 303–310.

Oda, S., Funato, H., Adachi-Akahane, S., Ito, M., Okada, A., Igarashi, H., … Kuroda, M. (2010). Dopamine D5 receptor immunoreactivity is differentially distributed in GABAergic interneurons and pyramidal cells in the rat medial prefrontal cortex. *Brain Research*, *1329*, 89–102.

Oda, S., Funato, H., Sato, F., Adachi-Akahane, S., Ito, M., Takase, K., & Kuroda, M. (2014). A subset of thalamocortical projections to the retrosplenial cortex possesses two vesicular glutamate transporter isoforms, VGluT1 and VGluT2, in axon terminals and somata. *Journal of Comparative Neurology*, *522*(9), 2089–2106.

Oda, S., Kuroda, M., Kakuta, S., & Kishi, K. (2001). Differential immunolocalization of m2 and m3 muscarinic receptors in the anteroventral and anterodorsal thalamic nuclei of the rat. *Brain Research*, *894*(1), 109–120.

Oda, S., Sato, F., Okada, A., Akahane, S., Igarashi, H., Yokofujita, J., … Kuroda, M. (2007). Immunolocalization of muscarinic receptor subtypes in the reticular thalamic nucleus of rats. *Brain Research Bulletin*, *74*(5), 376–384.

Pafundo, D. E., Miyamae, T., Lewis, D. A., & Gonzalez-Burgos, G. (2013). Cholinergic modulation of neuronal excitability and recurrent excitation-inhibition in prefrontal cortex circuits: implications for gamma oscillations. *The Journal of Physiology*, *591*(19), 4725–4748.

Paxinos, G., & Watson, C. (1998). *The rat brain in stereotaxic coordinates* (4th ed.). San Diego, CA: Academic Press.

Perederiy, J. V., Luikart, B. W., Washburn, E. K., Schnell, E., & Westbrook, G. L. (2013). Neural injury alters proliferation and integration of adult-generated neurons in the dentate gyrus. *Journal of Neuroscience*, *33*(11), 4754–4767.

Purrier, N., Engeland, W. C., & Kofuji, P. (2014). Mice deficient of glutamatergic signaling from intrinsically photosensitive retinal ganglion cells exhibit abnormal circadian photoentrainment. *PLoS One*, *9*(10), e111449.

Robinson, S. (2001). Changes in the cellular distribution of glutamine synthetase in Alzheimer's disease. *Journal of Neuroscience Research*, *66*(5), 972–980.

Rotaru, D. C., Barrionuevo, G., & Sesack, S. R. (2005). Mediodorsal thalamic afferents to layer III of the rat prefrontal cortex: Synaptic relationships to subclasses of interneurons. *Journal of Comparative Neurology*, *490*(3), 220–238.

Sarter, M., Parikh, V., & Howe, W. M. (2009). Phasic acetylcholine release and the volume transmission hypothesis: time to move on. *Nature Reviews Neuroscience*, *10*(5), 383–390.

Seamans, J. K. (2004). Working memory in prefrontal cortex and its neuromodulation. In S. Otani (Ed.), *Prefrontal cortex: from synaptic plasticity to cognition* (pp. 33–60). Boston, MA: Kluwer Academic Publishers.

Schildge, S., Bohrer, C., Beck, K., & Schachtrup, C. (2013). Isolation and culture of mouse cortical astrocytes. *Journal of Visualized Experiments*, *71*, e50079.

Shelton, M. K., & McCarthy, K. D. (2000). Hippocampal astrocytes exhibit Ca2+-elevating muscarinic cholinergic and histaminergic receptors in situ. *Journal of Neurochemistry*, *74*(2), 555–563.

Shin, J. D., & Jadhav, S. P. (2016). Multiple modes of hippocampal-prefrontal interactions in memory-guided behavior. *Current Opinion in Neurobiology*, *40*, 161–169.

Shirey, J. K., Brady, A. E., Jones, P. J., Davis, A. A., Bridges, T. M., Kennedy, J. P., … Conn, P. J. (2009). A selective allosteric potentiator of the M1 muscarinic acetylcholine receptor Increases activity of medial prefrontal cortical neurons and restores impairments in reversal learning. *Journal of Neuroscience*, *29*(45), 14271–14286.

Sidiropoulou, K., Pissadaki, E. K., & Poirazi, P. (2006). Inside the brain of a neuron. *EMBO Reports*, *7*(9), 886–892.

Siembab, V. C., Gomez-Perez, L., Rotterman, T. M., Shneider, N. A., & Alvarez, F. J. (2016). Role of primary afferents in the developmental regulation of motor axon synapse numbers on Renshaw cells. *Journal of Comparative Neurology*, *524*(9), 1892–1919.

Sofroniew, M. V., & Vinters, H. V. (2010). Astrocytes: Biology and pathology. *Acta Neuropathologica*, *119*(1), 7–35.

Steriade, M., & Buzsáki, G. (1990). Parellel activation of thalamic and cortical neurons by brainstem and basal forebrain cholinergic systems. In M. Steriade & D. Biesold (Eds.), *Brain cholinergic systems* (pp. 3–47). Oxford: Oxford University Press.

Stocker, M., & Pedarzani, P. (2000). Differential distribution of three Ca2+-activated K+ channel subunits, SK1, SK2, and SK3, in the adult rat central nervous system. *Molecular and Cellular Neuroscience*, *15*(5), 476–493.

Tabata, H. (2015). Diverse subtypes of astrocytes and their development during corticogenesis. *Frontiers in Neuroscience*, *9*(APR), 1–7.

Tabor, K. M., Wong, R. O. L., & Rubel, E. W. (2011). Topography and morphology of the inhibitory projection from superior olivary nucleus to nucleus laminaris in chickens (Gallus gallus). *Journal of Comparative Neurology*, *519*(2), 358–375.

Takata, N., Mishima, T., Hisatsune, C., Nagai, T., Ebisui, E., Mikoshiba, K., & Hirase, H. (2011). Astrocyte calcium signaling transforms cholinergic modulation to cortical plasticity in vivo. *Journal of Neuroscience*, *31*(49), 18155–18165.

Thurley, K., Senn, W., & Lüscher, H.-R. (2008). Dopamine increases the gain of the input-output response of rat prefrontal pyramidal neurons. *Journal of Neurophysiology*, *99*(6), 2985–2997.

Trantham-Davidson, H., Neely, L. C., Lavin, A., & Seamans, J. K. (2004). Mechanisms underlying differential D1 versus D2 dopamine receptor regulation of inhibition in prefrontal cortex. *Journal of Neuroscience*, *24*(47), 10652–10659.

van der Zee, E. A., de Jong, G. I., Strosberg, A. D., & Luiten, P. G. M. (1993). Muscarinic acetylcholine receptor-expression in astrocytes in the cortex of young and aged rats. *Glia*, *8*(1), 42–50.

Vogt, B. A. (2014). Cingulate cortex and pain architecture. In G. Paxinos (Ed.), *The rat nervous system* (4th ed., pp. 575–599). Amsterdam: Elsevier Academic Press.

Wainer, B. H., & Mesulam, M. M. (1990). Ascending cholinergic pathways in the rat brain. In M. Steriade & D. Biesold (Eds.), *Brain cholinergic systems* (pp. 65–119). Oxford: Oxford University Press.

Walz, W., & Lang, M. K. (1998). Immunocytochemical evidence for a distinct GFAP-negative subpopulation of astrocytes in the adult rat hippocampus. *Neuroscience Letters*, *257*(3), 127–130.

Wang, X., & Sun, Q. Q. (2012). Characterization of axo-axonic synapses in the piriform cortex of Mus musculus. *The Journal of Comparative Neurology*, *520*(4), 832–847.

Wässle, H., Regus-Leidig, H., & Haverkamp, S. (2006). Expression of the vesicular glutamate transporter vGluT2 in a subset of cones of the mouse retina. *Journal of Comparative Neurology*, *496*(4), 544–555.

Wilhelmsson, U., Bushong, E. A., Price, D. L., Smarr, B. L., Phung, V., Terada, M., … Pekny, M. (2006). Redefining the concept of reactive astrocytes as cells that remain within their unique domains upon reaction to injury. *Proceedings of the National Academy of Sciences of the United States of America*, *103*(46), 17513–17518.

Yang, Z., & Wang, K. K. W. (2015). Glial fibrillary acidic protein: From intermediate filament assembly and gliosis to neurobiomarker. *Trends in Neurosciences*, *38*(6), 364–374.

Yamasaki, M., Matsui, M., & Watanabe, M. (2010). Preferential localization of muscarinic M1 receptor on dendritic shaft and spine of cortical pyramidal cells and its anatomical evidence for volume transmission. *The Journal of Neuroscience*, *30*(12), 4408–4418.

Yao, W. D., Spealman, R. D., & Zhang, J. (2008). Dopaminergic signaling in dendritic spines. *Biochemical Pharmacology*, *75*(11), 2055–2069.

Yi, F., Ball, J., Stoll, K. E., Satpute, V. C., Mitchell, S. M., Pauli, J. L., … Lawrence, J. J. (2014). Direct excitation of parvalbumin-positive interneurons by M_1 muscarinic acetylcholine receptors: Roles in cellular excitability, inhibitory transmission and cognition. *The Journal of Physiology*, *592*(16), 3463–3494.

Zaborszky, L., Csordas, A., Mosca, K., Kim, J., Gielow, M. R., Vadasz, C., & Nadasdy, Z. (2015). Neurons in the basal forebrain project to the cortex in a complex topographic organization that reflects corticocortical connectivity patterns: An experimental study based on retrograde tracing and 3D reconstruction. *Cerebral Cortex*, *25*(1), 118–137.

Zhou, M., Schools, G. P., & Kimelberg, H. K. (2000). GFAP mRNA positive glia acutely isolated from rat hippocampus predominantly show complex current patterns. *Molecular Brain Research*, *76*(1), 121–131.

How to cite this article: Oda S, Tsuneoka Y, Yoshida S, et al. Immunolocalization of muscarinic M1 receptor in the rat medial prefrontal cortex. *J Comp Neurol*. 2018;526:1329–1350. https://doi.org/10.1002/cne.24409